Production and Characterization of Synthetic ErbB2 Virosomes for Vaccination Against Breast Cancer

Production and Characterization of Synthetic ErbB2 Virosomes for Vaccination Against Breast Cancer

Alexander (Sasha) G. Stafford

A Thesis in the Field of Biotechnology

for the Degree of Master of Liberal Arts in Extension Studies

Harvard University

March 2018

Abstract

Virosomes, lipid-based nanoparticles incorporating influenza surface proteins hemagglutinin (HA) and neuraminidase (NA), are an attractive biomimetic delivery system to stimulate the MHC I adaptive immune system. In contrast to conventional virosome preparations which are derived from live virus, here we describe the manufacture and characterization of synthetic virosomes incorporating recombinant HA and NA. A synthetic virosome production scheme represents a significant advance in the safety profile of this antigen delivery technology. To extend this approach to the production of a potent vaccine against breast cancer, the antigen ErbB2, the chemokine GM-CSF, and two lipid-based adjuvants (OxPAPC and MPLA) were incorporated into the virosome nanoparticles. As to the best of our knowledge, this is the first report of this approach, three different lipid formulations were evaluated to determine the incorporation efficacy of each component. The three lipid formulations evaluated were cholesterol combined with either anionic (DOPG), neutral (DOPC), or cationic (DOTAP) unsaturated-lipids. Analysis of intact virosomes revealed the presence of HA, NA, and OxPAPC on the exterior of the lipid nanoparticles. Further analysis, using disrupted virosomes, revealed that all six components were incorporated into DOPC and DOPG virosomes, with the greatest content found in DOPG virosomes for most constituents. These DOPC and DOPG virosomes were found to exhibit acceptable stability through 28 days of study as evaluated by dynamic light scattering, DOTAP virosomes displayed a

continual increase in size through 28 days of study. The successful incorporation of all six components and acceptable stability of DOPC and DOPG virosomes represents a significant advance in virosomal safety and nanoparticle complexity.

Acknowledgments

I would like to acknowledge and thank my loving wife, Caitlin, and my family for their unwavering support through this work. I would also like to thank Professor David Mooney for his mentorship and guidance through this project. I am grateful to my numerous instructors during this master's degree coursework, many of whom have influenced the scope of this project as well as contributed to my career advancement and research capabilities. Finally, I would like to acknowledge and thank my colleague Ed Doherty for his trust and support through our tenure together. Thank you all.

Table of Contents

List of Tables

List of Figures

Chapter I

Introduction

Vaccination is regarded as one of the most successful public health measures to date, having been utilized for more than 200 years (Greenwood, 2014). Based on 2013 projections from the Vaccines for Children (VFC) program, which was initiated in the United States in 1994, it has been estimated that vaccinations will prevent "21 million hospitalizations, and 732,000 deaths over the course of their lifetime" for people born between 1994 and 2013 (Whitney, 2014).

Historically, live attenuated vaccines were first developed by Edward Jenner in 1798 for the treatment of small pox, realizing that an animal poxvirus (cowpox) might have reduced potency in humans. With the turn of the 19th century, several physical and chemical methods had been developed to produce live attenuated and whole killed organisms, thus enabling vaccines against Rabies, Cholera, and the Plague. Then during the 20th century, the use of cell culture and purified proteins and polysaccharides provided the technical means to greatly increase the number of vaccines available to the public (Plotkin, 2014). Today, empowered with a greater understanding of the immune system, researchers are leveraging genetic engineering, nanotechnology, and biomaterial-based approaches to specifically target dendritic cells (DCs), the most efficacious antigen-presenting cells (APCs) responsible for initial activation of the adaptive immune response, thus increasing the efficacy of immunization. Though vaccination has been

effective in the immunization against pathogens, as suggested above, immunization against cancer has remained a significant challenge, most likely due in part to the role of immune tolerance, which can be broken with a strong and sustained immune response against cells that the immune system recognize as self (Adamina, 2006).

This study built upon several recent technologies – including the advent of infection-mimicking scaffolds capable of recruiting and programming DCs (Ali, 2009), the immune-stimulating and Major Histocompatibility Complex I (MHC I) presentation attributes of virosomes (Adamina, 2006), and a new adjuvant combination composed of a pathogen associated molecular pattern (PAMP) and damage associated molecular pattern (DAMP) that has been shown to 'hyperactivate' DCs – to produce a strong and sustained immune response (Zanoni, 2016).

Dendritic Cells and Antigen Presentation

Dendritic cells constantly scan the body, searching for non-self-entities such as viruses, bacteria, non-self proteins, etc., as part of the innate immune system. With exposure to such agents, immature DCs become activated and mature as antigens are internalized and processed. Mature DCs migrate to a draining lymph node where antigens are presented to T-cells, leading to initiation of the adaptive immune response. DC uptake and presentation of antigens can lead to two different, non-exclusive, activations of the adaptive immune response (Banchereau, 2000).

Exogenous soluble antigens are taken up by DCs and processed via the endosome, leading to partial hydrolysis of the protein, resulting in peptide presentation on MHC II

receptors and stimulation of CD4+ helper T cells. In contrast, endogenous antigens produced in infected or cancerous cells are processed via the proteasome and transported to the endoplasmic reticulum where they become associated with MHC I molecules leading to the stimulation of CD8+ T cells (see Figure 1; Banchereau, 2000). Canonically, immunotherapies against cancer have focused on the generation of CD8+ T cells and the production of cytotoxic T lymphocytes (CTLs).

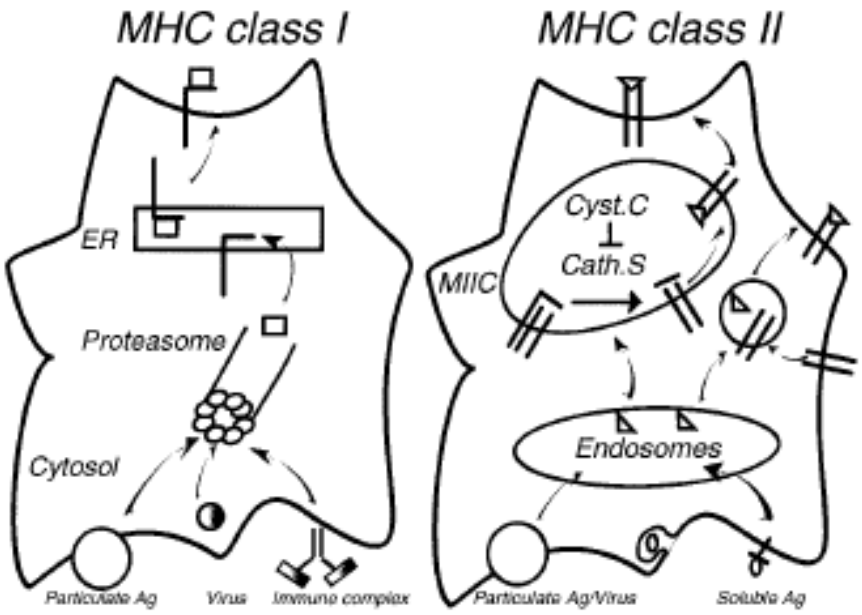

Figure 1: Schematic depicting antigen presenting cell processing of antigens via MHC I and II pathways "Dendritic cells load their major histocompatibility complex (MHC) molecules in multiple ways. (Left) MHC class I. Besides the classical endogenous pathway that loads peptides from self and intracellular pathogens, dendritic cells can also load MHC class I antigens through exogenous pathways with peptides originating from phagocytosed particulate antigens or immune complexes. Peptides are generated in the proteasome, transferred into the endoplasmic reticulum (ER), and loaded onto the nascent MHC class I molecules. (Right) MHC class II. Dendritic cells capture soluble antigen (Ag) either through macropinocytosis or receptor-mediated endocytosis. They also capture particles through phagocytosis. The antigens are subsequently degraded in endosomes, and the generated polypeptides are transported into the MHC class II–rich compartments (MIIC) for their loading onto the nascent MHC class II molecules while DCs mature. The invariant chain, associated with nascent MHC class II, is cleaved by cathepsin S (Cath.S), which in immature DCs is inhibited by cystatin C (Cyst.C). After maturation, cystatin C is downregulated, thereby releasing active cathepsin S. The HLA-DM molecules help the loading of peptides onto MHC class II molecules. A fraction of the peptides are loaded onto empty MHC class II molecules recycled from the cell surface (cycle on the right)." (Banchereau, 2000)

The Influenza Virus and Synthetic Virosomes

The influenza virus membrane contains two major membrane bound glycoproteins, hemagglutinin (HA) and neuraminidase (NA). Viral strains are named based on their respective serotypes (HA has 16 subtypes, NA 9 subtypes in humans). For example, H1N1 (responsible for the 1918 Spanish Flu pandemic) or H2N3 (responsible for the 1968 Hong Kong Flu), etc. (Blut, 2009).

Hemagglutinin is responsible for cellular docking and subsequent binding of the virus to the endosomal membrane, where it induces fusion and release of the viral nucleocapsid in the cytosol. Upon release of the nucleocapsid, eight viral RNA-segments are available for replication via associated polymerases (Blut, 2009). With newly formed virus particles, neuraminidase functions to prevent aggregation during budding and viral release. Further, NA cleaves sialic acid residues from the respiratory tract mucins facilitating the translocation of the virus to the target cells and may participate to some extent in cellular fusion (Shtyrya, 2009). Although the functions of NA are not necessary in the context of this thesis work, the protein was included in the proposed virosomes to maintain analogy to conventionally produced virosomes.

Virosomes, lipid bilayers (liposomes) containing viral – conventionally influenza virus – hemagglutinin and neuraminidase membrane glycoproteins present an attractive approach towards the immunization against cancer. Virosomes do not contain genetic material and are therefore non-pathological, yet they retain the ability to bind cell surface sialic acid residues via hemagglutinin. Upon binding, the virosome is internalized via receptor-mediated endocytosis, where the reduced pH of the endosome induces a

conformational change in HA allowing virosome-endosome fusion and release of the virosome cargo into the cytoplasm of the cell. Virosomes have become an attractive delivery device for the cytosolic release of drugs, proteins, as well as nucleotide-based therapies and gene editing technologies (Felnerova, 2004). Virosomes are also attractive immunomodulatory nanoparticles, shown to effectively stimulate both MHC I and MHC II presentation – via HA fusion and late endosomal/lysosomal (non-fusion) pathways, respectively – with a preference for MHC I, CD8+ T cell stimulation, and the production of CTLs (Bungener, 2002).

Traditionally, virosomes have been produced *ex vivo* through the harvesting of inoculated influenza cell lines. Culture media is then concentrated and purified by ultrafiltration and sucrose gradient ultracentrifugation, respectively. Collected virus membrane is then disrupted by dissolution with a short phospholipid (DCPC), with elimination of the nucleocapsid by ultracentrifugation and re-coalescence of the membrane fraction through dialysis (Abdoli, 2013). Although this process is laborious, the virosomes produced contain NA, and active HA glycoproteins. As virosomes contain natural phospholipids, they are biodegradable and have a low risk of toxicity.

With the recent commercial availability of recombinant HA and NA proteins (Sino Biologicals, Inc.), this thesis aimed to incorporate these proteins into a liposome-based manufacturing process. Liposomes represent the most successful therapeutic nanoparticle currently on the market, as measured by the number of approved products, due to their high biocompatibility and scalable production (Dua, 2012). Liposomes are easily manufactured through several different approaches, however, the most conventional is the thin film hydration method (see Appendix 6, Figure 51, for a

schematic), which produces lipid bilayers through the aqueous rehydration of dehydrated lipids, in the presence of drugs, biologics, or adjuvants. The lipid bilayer is then extruded through a nano-porous membrane to produce liposomes of uniform size. Any excess drug, biologic, or adjuvant is then eliminated through purification via dialysis against a buffer of choice. This process is relatively short and highly modular, making it an attractive drug delivery approach (Dua, 2012). This thesis aimed to extend this approach to the production of synthetic, recombinant HA and NA based virosomes.

As sialic acid residues are ubiquitous across mammalian cell surfaces, to effectively leverage virosomal processing against dendritic cells, there is a need to either target these virosomes to DCs or to enrich a site *in vivo* to enhance for DC populations. Although antibodies could be utilized for DC targeting, Ali, et. al. have shown that a biomaterial based scaffold can enrich for DCs *in situ* (2009). This approach combined a macro-porous PLGA implant and granulocyte-macrophage colony stimulating factor (GM-CSF), a potent cytokine capable of DC recruitment and activation in the presence of pro-inflammatory factors such as viral and bacterial infections (van de Laar, 2012), to enhance for populations of DCs within the scaffold structure. Dendritic cells were then exposed to adjuvant (CpG oligodeoxynucleotides, bacterial ssDNA) and antigen (autologous tumor lysate) within the scaffold structure to program them against melanoma tumors (Ali, 2009). GM-CSF has been implicated in the priming and effector stages of the immune response (Zarei, 2009), invoking both cell mediated and antibody responses (Mach, 2000). Although administration of exogenous GM-CSF helps to attenuate T regulatory cell tumor infiltrates, thought to be responsible for poor tumor immunogenicity, high doses of GM-CSF results in sub-optimal immunization through the

generation of immunosuppressive cells. To this point, localized and sustained release has been shown to potentiate the vaccination effect, as demonstrated using cells engineered to release nanogram quantities of GM-CSF daily (Serafini, 2004). Through a dose-evaluation study, Ali, et. al. (2009) determined that 3 mcg per scaffold was an optimal GM-CSF concentration for the PLGA *in situ* vaccine scaffold. As this thesis aimed to utilize GM-CSF as both an adjuvant and DC recruiting factor, further supplementation of GM-CSF may aid the rapid recruitment of DCs to a potential local scaffold, thus facilitating enrichment prior to virosome release.

Hyperactivating Dendritic Cells via Adjuvants

Upon exposure to immune-stimulating adjuvants (compounds capable of enhancing the immune response to antigens), DCs become activated, mature against the presented antigen, and migrate to draining lymph nodes. Adjuvants play a critical role in the programming of recruited immature DCs to antigens. Although only a few adjuvants have been approved by the FDA for commercial use, there are numerous adjuvants currently in clinical trials (Coffman, 2010). Many of the adjuvants currently under investigation are ligands for toll-like receptors (TLRs), a class of receptors that have broad recognition of pathogens as part of the innate immune system. Of particular interest here is the TLR4 receptor, which recognizes lipopolysaccharides (LPS) found in many gram-negative bacteria. LPS, a pathogen-associated molecular pattern (PAMP) and has long been investigated as an immune-stimulatory factor due to its ability to activate monocytes and macrophages. LPS has been previously incorporated into fusogenic

virosomes, where it was shown to exhibit approximately 10-fold greater activity than free LPS; similarly produced LPS containing liposomes were shown to be 100-fold less effective (Dijkstra, 1996).

Recently, Zanoni, et. al. (2016) described an adjuvant combination, LPS and OxPAPC, that was found to produce a previously unknown DC activation state – hyperactive – as opposed to conventional inactive and active states. OxPAPC is a damage-associated molecular pattern (DAMP) found in endogenous dying cells where it can reach concentration of 10-100 micromolar. Although OxPAPC is thought to be a LPS-mimic, Zanoni et. al. (2016) established that it does not activate TLR4 as LPS does. Instead, both LPS and OxPAPC activate caspase-11, an intracellular receptor protease also known as a non-canonical inflammasome, albeit via different binding domains. Activation of caspase-11 results in increased production of IL-1β, a potent cytokine that is a major contributor to inflammatory responses and apoptosis. LPS binding to caspase-11 results in pyroptosis and septic shock, while OxPAPC facilitates the formation of a caspase-1/11 hetero-complex with an absence of pyroptosis. Zanoni, et. al. (2016) concluded that the co-administration of LPS and OxPAPC facilitated the canonical DC activation state, while also promoting IL-1β release and DC survival, a so called *hyperactive* state. With such, hyperactive DCs release IL-1β for longer periods leading to sustained stimulation of memory T-cells. Prolonged DC survival is a provocative finding, as DCs have short lifespans (van de Laar, 2012), this hyperactive state may aid to alleviate some of the shortcomings of immunotherapy, such as the need for boosters (Saroja, 2011) or revaccination (thus increasing patient compliance). Although Zanoni, et. al. (2016) performed some work to evaluate the transfection of LPS and OxPAPC via

a DOTAP liposome complex, a natural extension of this research would be the co-administration in presence of antigen via virosomes, as was investigated here.

Although LPS is a potent stimulator of DCs and the immune system, LPS is highly toxic in humans, thus restricting its clinical application. A less toxic LPS analog, Monophosphoryl Lipid A (MPLA), has progressed through clinical trials and is an adjuvant in Cervarix™, an FDA approved vaccine for human papillomavirus (HPV) where it has safely been administered to thousands of patients (Oblak, 2011). MPLA is approximately 1,000 times less toxic than LPS, while maintaining comparable immunologic potency through the TRL4 receptor (Casella, 2008). With such, this study substituted LPS with the less toxic MPLA, in hopes of increasing the therapeutic window as part of preemptive translational efforts.

Antigen Presentation via Biomaterial Based Scaffolds

Ali, et. al. (2009) reported the incorporation of autologous tumor lysate as antigen in PLGA scaffolds to elicit sustained presentation, however these lysates are often significantly heterogeneous and often require substantial amounts of protein to elicit an immune response. This study used a defined antigen protein (ErbB2) to reduce the amount of antigen required, as well as to simplify the virosome encapsulation analytics. ErbB2 was used as a proof-of-concept model antigen, other antigen proteins could be incorporated into this virosome vaccine platform, thus enabling vaccination against further indications.

ErbB2, also known as Her2, is part of the epidermal growth factor receptor (EGFR) family and has been found to be overexpressed in several cancers, most notably in "20-30% of breast cancer tumors" (Mitri, 2012), where overexpression reaches 100x greater levels than that in non-cancerous cells. As non-cancerous cells express low levels of ErbB2, use of this protein as an antigen provides potential target specificity to the manifest cytotoxic T-cells against breast cancer, while minimizing off-target toxicity (Yarden, 2001). ErbB2 is a 185-kDa transmembrane protein, devoid of an extracellular ligand binding domain, however, it can form hetero-dimers with other EGFR members, where the ErbB2/ErbB3 dimer is thought to be neoplastic (Mitri, 2012). Although ErbB2 peptides have been previously used in immunization efforts, these peptides are often weakly immunogenic in humans (Salazar, 2003), thus this study utilized a recombinant extracellular domain (70 kDa, rErbB2) encapsulated for antigen presentation via virosomes. This rErbB2 does not contain the transmembrane domains, therefore the protein was anticipated to incorporated into the aqueous partition encapsulated within the lipid bilayer and was to be delivered to the cytosol for MHC I processing as described above. Further, as the larger antigen protein was used here, there is the potential to generate multiple MCH I – ErbB2 peptide presentations. As the MHC I presentation of ErbB2 is anticipated to be associated with CD8+ cytotoxic T lymphocytes generation, these cells should be maturated against endogenous breast cancer cells.

Synthesis

The proposed virosomes represent a novel approach to potentially stimulate a CTL mediated immune response towards ErbB2, a breast cancer associated protein. As many previous oncology vaccine approaches have failed to elicit significant responses, the proposed virosomes leverages multiple adjuvant systems to maximize immune stimulation. Subsequently, this system has the potential to be released from biomaterial-based scaffolds capable of controlled and sustained release, while simultaneously recruiting dendritic cells to the local environment of administration. In addition, this technology could be used in conjunction with checkpoint blockade antibodies to further potentiate this immunotherapy through the attenuation of regulatory T-cells. Finally, these virosomes, or variations thereof, could also be used for cytosolic drug delivery applications in oncology or beyond.

Chapter II

Research Approach

The battle against cancer is currently undergoing a significant paradigm shift with the advance of immuno-oncology, where the immune system is utilized to fight cancer. This is most recently exemplified by the success of CAR-T -- where autologous T-cells are manipulated to express chimeric antigen receptors -- as well as anti-PD-1/PD-L1, and anti-CTLA-4 therapies, so called immune checkpoint blockade inhibitors. These approaches have significantly shifted the Kaplan-Meier survival curve for many cancer indications (Hodi, 2010), allowing a subset of patients long-term survival without disease progression. In contrast to traditional chemotherapy, which has significant off-target toxicity, therapeutic cancer vaccination promises to increase therapeutic specificity while establishing immune memory against tumors, thus potentially providing resistance to recurrence and metastasis.

Autologous tumor cell vaccines were some of the first therapeutic vaccines to reach clinical trials and may be exemplified by the success of GVAX, a GM-CSF transduced tumor cell vaccine. While GVAX results in recruitment of dendritic cells and priming of $CD8^+$ T cells, it requires *ex vivo* irradiation and transfection, adding significant processing time and costs (Dranoff, 1993). To circumvent some of these limitations, in 2012, a Phase I clinical trial (NCT01753089) was initiated to program the immune system *in situ.* This was accomplished by exposing dendritic cells to autologous

tumor lysate in the presence of GM-CSF (a cytokine) and CpG (a Toll-like Receptor 9 agonist) released from a poly(lactic-co-glycolic acid) (PLGA) macro-porous scaffold implanted subcutaneously. The preclinical data generated using this *in situ* approach demonstrated it surpassed GVAX efficacy in a head to head comparison (Ali, 2009). Although this approach holds great promise, it would be clinically advantageous to have an injectable version of this *in situ* cancer vaccine while further potentiating the immune-stimulating effect against the antigen target.

This thesis aimed to leverage the MHC I presentation potential of virosomes (Adamina, 2006), to deliver antigen for the potential treatment of breast cancer. The immune-stimulating effect of these nanoparticles were further augmented by integration of a recently described adjuvant combination of lipopolysaccharide (a bacterial endotoxin) and OxPAPC (an oxidized lipid presented on the surface of cells after damage) that has been found to hyper-activate dendritic cells (Zanoni, 2016). These virosomes could be used to vaccinate against a defined antigen, ErbB2 to generate cytotoxic T lymphocytes capable of infiltrating and destroying breast cancer tumors.

Virosomes, have been traditionally produced using reconstituted viral particles (Abdoli, 2013). Recently the influenza membrane proteins, HA and NA, have become commercially available, enabling the rapid production and development of virosomal formulations through liposomal production processes – e.g. thin film rehydration (see Supplemental Figure 27). These synthetic virosomes would lack any exposure to viral DNA, thus significantly reducing safety concerns associated with the potential for residual pathogenicity. Through localized, sustained release of virosomes, it is hypothesized that this configuration would provide an injectable *in situ* $CD8^+$

potentiating vaccine against the ErbB2 antigen for the treatment of breast cancer. This thesis aimed to evaluate the ability to produce the proposed virosomes using three different lipid combinations (DOPC, DOPG, or DOTAP and Cholesterol; see Supplemental Figures 22-25) in order to assess potential incorporation differences between lipid charges.

Specifically, the lipid soluble DC stimulating factors (MPLA and OxPAPC) were added to the lipid/cholesterol mixture prior to drying. The protein factors – influenza hemagglutinin (HA) and neuraminidase (NA), the DC recruitment factor (GM-CSF), and the breast cancer associated antigen (rErbB2) – were incorporated into the virosome structure during thin-film rehydration. The six bioactive compounds were incorporated into three different lipid bilayer compositions, which vary in charge, either 1:1 molar ratios of DOTAP:Cholesterol (cationic), DOPC:Cholesterol (Neutral), and DOPG:Cholesterol (Anionic). DOTAP, DOPC, and DOPG are all unsaturated lipids of equal length and unsaturation (9Z), varying in the polarity of the head group.

Unsaturated lipids and cholesterol have been selected here to reduce the lipid bilayer phase transition temperature (T_g) during the extrusion process. This reduced T_g was anticipated to avoid denaturation of the incorporated proteins ErbB2, GM-CSF, HA, and NA. Studies examining the ratio of lipids and cholesterol in liposomes have revealed that formulations with equimolar ratios between unsaturated-lipids and cholesterol exhibit the greatest stability *in vitro* and *in vivo* (New, 1994). Liposomes or virosomes created solely from these unsaturated-lipids would be expected to exhibit significant permeability, due to solvent accessible space created by the kink in the lipid tail. This permeability is significantly reduced through the addition of cholesterol, as it helps to fill

in this space, thus increasing the retention of encapsulated cargo (drugs, biologics, etc.; New, 1994).

In this study, the hemagglutinin precursor protein (HA_0) was incorporated into the lipid bilayer via its trans-membrane domain. Trypsin-like serine endoproteases produced in response to infection, or secreted by bacteria, and the cells of the human respiratory tract can cleave the HA_0 protein into the mature disulfide-bonded HA_1 and HA_2 proteins (Klenk, 1994). Though HA_0 can facilitate receptor binding (Wiley, 1987), cleavage is required for virus pathogenicity and is found to vary with differences in glycosylation (where glycosylation can interfere with post-translational processing) and presence and number of positive amino acids (arginine and lysine) in the cleavage site (Webster, 1987). A trend towards reduced glycosylation and greater number of positive amino acids results in increased pathogenicity (Chen, 1998; Klenk, 1994). Cleavage of HA confers the protein with the low pH sensitivity required to induce the irreversible conformational change (Chen, 1998) needed for endosomal membrane fusion (Skehel, 1982).

As this study ultimately aimed to produce an infection-mimicking microenvironment, HA_0 was used as an experimental proof of concept with the assumption that it could be readily cleaved through extracellular protease activity. This potential delay in activation may be an asset of the proposed system, as it may allow sufficient populations of DCs to be recruited to the administration site prior to virosomal fusogenic activation, thus allowing a temporally controlled enrichment of the target cell population (DCs). Further development could be performed to optimize the fusogenicity through either use of more virulent strains of influenza (H5 and H7; Senne, 1996), use of pre-cleaved HA_0 recombinant proteins, or pretreatment of HA_0 with trypsin *ex vivo* to

generate HA_1 and HA_2 (Klenk, 1975). Once activated, HA facilitates cellular fusion through the binding of terminal sialic acid residues on cell surface receptors (Wiley, 1987).

Systemic administration of lipid-based nanoparticles can often accumulate in the reticuloendothelial system (RES; liver, spleen, and lungs), where there is the potential for localized toxicity in said organs (Keneda, 2000). Systemic toxicity can often be significantly reduced through localized, sustained release of these nanoparticles to target environments. Further, as therapeutic administration is proximal to the target, often lower doses are required to achieve comparable efficacy to that of systemic administration. Though direct intratumoral injection of liposomes or virosomes is possible, these nanoparticles are often cleared from the tumor within days (Harrington, 2000). As localized and sustained delivery of vaccines maximize the immune response (Mach, 2000), the virosomes produced via this thesis could subsequently be released through several biopolymer-based drug delivery systems – as has been previously demonstrated for liposomes (Grijalvo, 2016).

Biopolymer based hydrogels, hydrophilic network of polymer chains, have long been an attractive potential scaffold for the delivery of lipid-based nanoparticles. However, they have often been found to produce sub-optimal release kinetics due to an inability to limit diffusion, while also suffering from heterogeneous distributions (Grijalvo, 2016). Further, many biopolymers are degraded in the human body through endogenous enzymes, which can result in significant variability in both their release and degradation kinetics across tissues due to differences in local enzyme concentrations.

Alginate, a biopolymer derived from brown algae, which lacks a human enzyme to break it down, can be chemically oxidized to invoke degradation through pH mediated hydrolysis (Bouhadir, 2001). Alginate hydrogels have a long history of use for protein and cellular encapsulation due to their significant hydrophilicity, ability to crosslink under mild conditions, and their similarity to the extracellular matrix (ECM) in both water content and mechanical properties. With such, biopolymer-based hydrogels are generally regarded as highly biocompatible, non-inflammatory, and biodegradable (Drury, 2003).

A recently developed injectable bio-orthogonal click-alginate hydrogel (Desai, 2015) is an attractive candidate to deliver antigen loaded virosomes capable of stimulating the immune system against ErbB2. These hydrogels offer a means by which to modulate the cross-linking density of these networks, thus allowing for the potential retention of lipid-based nanoparticle (liposomes and virosomes) without interaction with encapsulated cargo. Using oxidized alginate (Bouhadir, 2001), this approach could lead to degradation mediated (diffusion limited) release of encapsulated virosomes through the pH mediated hydrolysis.

Although the described virosomes would potentially be applied to breast cancer using the ErbB2 antigen, the foundational configuration of virosome presented in this work (lipid, cholesterol, GM-CSF, HA, and NA) could easily accommodate other adjuvants, most notability bacterial dsRNA such as CpG or Poly I:C via cationic DOTAP electrostatic loading (Talesh, 2016), and/or other peptide, protein, or lipopolysaccharide antigens. By using either defined, or lysate derived antigens, this platform technology could be expanded for use in non-oncology applications such as bacterial, viral, and

parasitic infections, other disease states (such as Alzheimer's, hypertension, obesity, etc.), or drugs of abuse (e.g. cocaine, morphine, etc.). Further, these virosomes (without GM-CSF and adjuvants) could also be used for conventional small molecule, biologic, and nucleotide based cytosolic drug delivery.

Chapter III

Materials and Methods

Given the complexity of the manufactured virosomes, several analytical methods were employed to establish relative content values across the three lipid formulations evaluated. Among these were intact and disruptive ELISAs, SEC analysis, DLS, Zeta Potential, MUNANA activity assay, EndoSafe Endotoxin testing, and a micro-BCA assay. These assays are described as follows:

Enzyme-linked immunosorbent assay (ELISA) is a common analytical technique used to quantify antibody responses as well as analytes with high sensitivity, often reaching the picogram per milliliter (pg/mL) range (Engvall, 1971). ELISAs are often used as an analytical proxy for bioactivity, as each assay is highly specific for native protein confirmations through the use of epitope specific antibodies. Although there are many types of ELISAs commercially available, this work leveraged a series of sandwich ELISAs for the quantification of several proteins. In general sandwich ELISAs consist of a 96-well plate on to which a capture antibody specific for the analyte has been adsorbed. After excess antibody has been removed, diluted analyte is added and incubated. Analyte is then removed, and a detection antibody is added and incubated. The detection antibody is often directly labeled with a fluorophore or conjugated with horseradish peroxidase (HRP). The antibody-HRP conjugate will enzymatically convert a substrate (e.g. TMB – 3,3’,5,5’-Tetramethylbenzidine) to a colored product in the presence of hydrogen

peroxide in direct proportion to the amount of analyte captured. Similarly, fluorescent intensity of the detection antibody fluorophore conjugate can be used to quantify captured analyte.

Size Exclusion Chromatography (SEC) is a common protein characterization technique that separates analytes based on size (Hong, 2012) via High Performance Liquid Chromatography (HPLC). This analytical method was extended here to the analysis of virosomes as a method to separate virosome-antibody complexes from free antibody. The porous columns used in SEC are often polyacrylamide based and can be purchased with different particle sizes and pore diameters. As analytes are introduced into the column(s), smaller compounds are able to enter the pores where they are retained and take time to exit the matrix, this process recurs as the analyte progresses along the column. In contrast, larger compounds are not as readily able to enter the pores or can be excluded entirely if large enough, exhibit shorter residence time in the column(s). Although secondary interactions can occur, these are often minimized through the addition of salts, or sucrose as was used here. In general, these differences in matrix interactions lead to larger molecules eluting earlier and smaller analytes eluting later in chromatograms.

Dynamic Light Scattering (DLS) is an analytical method used to determine the size of particles in a liquid. The method determines the Brownian motion (or the translational diffusion coefficient) of the analyte in solution, from which the hydrodynamic radius of the particle can be determined through the Stokes-Einstein equation (Hassan, 2015). Multiple determinations of analyte size produce a profile, which enables the determination of the PolyDispersity Index (PDI). The PDI ranges from 0 to 1,

with greater values reflecting more polydisperse particles and lower values reflecting more monodisperse particle solutions.

The evaluation of particle charge was determined by Zeta Potential, a measure of the electrophoretic mobility of a particle. With an electric current applied, the particle surface charge is evaluated against its dispersion liquid to determine the zeta potential. In the evaluation of nanoparticles, values close to neutral are considered unstable, while larger values are considered more stable due to potential electrostatic repulsion between particles (Clogston, 2011).

The MUNANA assay for neuraminidase activity is a long-standing, fluorometric assay (Potier, 1979) for viral titration and determination of efficacy of neuraminidase inhibitors (Wetherall, 2003). The assay uses a fluorophore-carbohydrate conjugate that is hydrolyzed by NA enzymatic activity. The fluorophore product provides a quantitative assessment of NA content via endpoint fluorescence. In this case incubation was extended overnight due to the relatively low NA content in comparison to whole influenza virus.

The EndoSafe assay kit is a product developed by Charles River Laboratories and is a FDA approved testing method for the determination of endotoxin. The assay uses Limulus Amebocyte Lysate (LAL) reagents and chromogenic substrates preloaded into microfluidic channels to rapidly quantitate endotoxin sample levels in proportion to substrate color change (Gee, 2008). As MPLA is a LPS mimetic, this assay was extended to the evaluation of MPLA content in virosomes. To minimize potential false positives, endotoxin free reagents and water were used across all virosome formulations.

The micro-BCA assay is conventional colorimetric assay for the determination of total protein concentration. The BCA assay relies on the reduction of copper via the peptide amide bond to produce a colored product via chelation of bicinchoninic acid molecules. Upon chelation, the solution changes from green to purple in proportion to the number of amides present in the sample (Olson, 2007).

Reagents

Endotoxin free Sucrose was acquired from EMD Millipore. Chloroform, Cholesterol, HEPES, MUNANA, and Triton X-100 were obtained from Sigma-Aldrich. DOPC, DOPG, DOTAP, anti-OxPAPC-biotin-E06 antibody conjugate, and anti-OxPAPC-TopFluor-E06 antibody were procured from Avanti Lipids. MPLA and OxPAPC were obtained from InvivoGen. Sodium chloride and Bovine Serum Albumin (BSA) were purchased from VWR. Endotoxin free water was obtained from a Milli-Q system, while PBS and Water for Injection (WFI) were obtained from Lonza. EndoSafe endotoxin testing kits were procured from Charles River Laboratories. The Micro-BCA assay kit was acquired from Thermo Scientific. GM-CSF and ErbB2 ELISA kits, streptavidin-HRP conjugate, and ELISA development reagents were purchased from R&D Systems. HA (H1N1 - A/California/04/2009), NA (H1N1), and ErbB2 proteins as well as HA ELISA kits were acquired from Sino Biologicals. Murine GM-CSF was obtained from Peprotech. Anti-NA-FITC antibody conjugate was procured from Biorbyt.

Preparation of Liposome Controls

Liposome controls were prepared by combining 100 mcL of Cholesterol (25 mg/mL in chloroform), and either 49 mcL DOPC (25 mg/mL in chloroform), 49 mcL DOPG (25 mg/mL in chloroform), or 55 mcL DOTAP (25 mg/mL in chloroform); see Appendix 4, Supplemental Figures 22-25, for lipid molecular structures. The solution was mixed and evaporated overnight *in vaco*. The resulting thin film was rehydrated with 1 mL of 10% sucrose, 20 mM HEPES, pH 7.3 and sonicated 10 x 1 seconds in a bath sonicator. The solution was then extruded through a 100-nm polycarbonate (PC) membrane using a mini extruder (Avanti Lipids, Inc.). Samples were then dialyzed using 100 kDa molecular weight cut-off (MWCO) Float-A-Lyzer G2 devices (Spectrum Labs Cat #G235035) against 5 liters of 10% sucrose, 20 mM HEPES, pH 7.3 for 2 days with an overnight diluent change. All liposome control lots were produced and processed in parallel to minimize processing differences across formulations. The product was stored at 2-8^{o} C between uses.

Preparation of Adjusomes (Adjuvant loaded Liposomes)

Adjuvant loaded liposomes were prepared by combining 100 mcL of Cholesterol (25 mg/mL in chloroform), 88 mcL MPLA (1 mg/mL in chloroform), 42 mcL OxPAPC (1 mg/mL in chloroform) and either 49 mcL DOPC (25 mg/mL in chloroform), 49 mcL DOPG (25 mg/mL in chloroform), or 55 mcL DOTAP (25 mg/mL in chloroform). The solution was mixed and evaporated overnight *in vaco*. The resulting thin film was

rehydrated with 1 mL of 10% sucrose, 20 mM HEPES, pH 7.3 and sonicated 10 x 1 seconds in a bath sonicator. The solution was then extruded through a 100 nm PC membrane using a mini extruder (Avanti Lipids, Inc.). Samples were then dialyzed using 100 kDa MWCO Float-A-Lyzer G2 devices (Spectrum Labs Cat #G235035) against 5 liters of 10% sucrose, 20 mM HEPES, pH 7.3 for 2 days with an overnight diluent change. All adjusome lots were produced and processed in parallel to minimize processing differences across formulations. The product was stored at 2-8^{o} C between uses.

Preparation of Virosomes

Virosomes were prepared by combining 100 mcL of Cholesterol (25 mg/mL in chloroform), 88 mcL MPLA (1 mg/mL in chloroform), 42 mcL OxPAPC (1 mg/mL in chloroform) and either 49 mcL DOPC (25 mg/mL in chloroform), 49 mcL DOPG (25 mg/mL in chloroform), or 55 mcL DOTAP (25 mg/mL in chloroform). The solution was mixed and evaporated overnight *in vaco*. Lyophilized vials of HA, NA, and ErbB2 were reconstituted using 10% Sucrose, 20 mM HEPES, pH 7.3 and allowed to mix at room temperature for 20 minutes prior to use. GM-CSF (1 mg) had been previously reconstituted with 1 mL of WFI and allowed to mix at room temperature for 20 minutes prior to use. The thin film was then rehydrated with 100 mcL HA (200 mcg/mL), 80 mcL NA (150 mcg/mL), 20 mcL GM-CSF (1 mg/mL), 100 mcL ErbB2 (400 mcg/mL), and 700 mcL 10% sucrose, 20 mM HEPES, pH 7.3 and sonicated 10 x 1 seconds in a bath sonicator. The solution was then extruded through a 100-nm PC membrane using a mini

extruder (Avanti Lipids, Inc.). Samples were then dialyzed using 100 kDa MWCO Float-A-Lyzer G2 devices (Spectrum Labs Cat #G235035) against 5 liters of 10% sucrose, 20 mM HEPES, pH 7.3 for 2 days with an overnight diluent change. All virosome lots were produced and processed in parallel to minimize processing differences across formulations. The product was stored at 2-8^{o} C between uses.

Determination of Size, Polydispersity Index, and Zeta Potential

Liposome and virosomes samples were diluted 20x by combining 35 mcL sample with 665 mcL 10 mM NaCl and the solution was transferred to a disposable folded capillary cell (Malvern Cat #DTS1070). Samples were analyzed on a Nano Zetasizer (Malvern Instruments, Ltd.) for Size and Zeta Potential according to manufacturer protocols.

Micro BCA Assay for Determination of NA Vial Content

Sino Biologicals supplies NA with a 200U label claim, rather than a mass, therefore a Micro-BCA assay was conducted to determine an approximate concentration after reconstitution with 1 mL 10% Sucrose, 20 mM HEPES, pH 7.3. NA stock was diluted 50x by combining 20 mcL with 980 mcL PBS. A standard curve using BSA was established by diluting 2 mg/mL stock to 200 mcg/mL and then conducting 2x serial dilutions thereafter using PBS. The assay was conducted in accordance with manufacturer protocol (Thermo Scientific Cat #23235), using a BCA working solution of

25A:24B:1C. Standards and samples were plated using 100 mcL per well combined with 100 mcL of BCA working solution, the plate was covered and incubated at 37 ºC for 2 hours and the optical density was read at 562 nm on a Synergy H1 Plate Reader (BioTek Instruments, Inc.).

EndoSafe Determination of MPLA Content

Virosome samples – DOPC and DOPG – were disrupted by combining 10 mcL sample with 10 mcL 1% w/v Triton X-100 and sonicating for 5 minutes. Samples were diluted to 50x through addition of 480 mcL WFI, samples were then sonicated for 5 minutes. Samples were subsequently diluted to bring endotoxin values within the EndoSafe cartridge dynamic range (0.5-0.005 EU/mL). DOPC and DOPG virosome formulations were diluted to 2500x by combining 20 mcL of 50x dilution with 980 mcL WFI. DOPG formulations were further diluted to 25000x by combining 100 mcL of 2500x dilution and 900 mcL WFI. DOPC liposome controls and DOTAP virosome samples were diluted to 10x by disrupting 15 mcL virosome sample with 15 mcL 1% w/v Triton X-100 and sonicating for 5 minutes. Samples were diluted to 50x by adding 120 mcL WFI and sonicating for 5 minutes. DOPG and DOTAP liposome controls were diluted 100x by combining 10 mcL sample with 10 mcL 1% Triton X-100 and sonicating for 5 minutes, 980 mcL WFI was then added and samples were sonicated again for 5 minutes. Samples and controls were analyzed via EndoSafe kits (Charles River Laboratories, Cat #PTS55005F) according to manufacturer protocols. Briefly, 25 mcL of

diluted samples were added to sample and control wells and the assay was run on a EndoSafe – Multi-Cartridge System (Charles River Laboratories).

Intact Virosome Sandwich ELISA for OxPAPC Content

Virosome samples were diluted to 50x by combining 20 mcL sample with 980 mcL PBS w/ 1% BSA. An intact virosome sandwich ELISA was conducted by adding 100 mcL of samples to a HA Sandwich ELISA kit (Sino Biological Cat #KIT11055) and incubating overnight at room temperature. The plate was then aspirated and washed 5x with wash buffer and decanted. The E06 detection antibody (OxPAPC-biotin; Avanti Lipids Cat #330002) was diluted to 1 mcg/mL in HA dilution buffer and 100 mcL was added to wells and incubated at room temperature for 2 hours. The plate was then aspirated, washed 5x with wash buffer, and decanted. The streptavidin-HRP conjugate (R&D Systems Cat #DY998) was diluted 50x in PBS w/ 1% BSA and 100 mcL was added to each well and incubated for 45 minutes. The plate was then aspirated, washed 5x with wash buffer, and decanted. Substrate Solution (200 mcL; R&D Systems Cat #DY999) was added to each well and the plate was incubated in the dark at room temperature for approximately 45 minutes. Stop Solution, 50 mcL, was added to each well and the optical density was read at 450 nm and 570 nm (reference wavelength) on a Synergy H1 Plate Reader (BioTek Instruments, Inc.).

SEC of Virosomes for OxPAPC Content

Virosome sample were diluted by combining 25 mcL with 100 mcL 10% Sucrose, 20 mM HEPES, pH 7.3 and 1 mcL TopFluor-E06 Antibody. Samples were analyzed via SEC using G5000PWxl and G6000PWxl columns in series (Tosoh, Cat #08023 and 08024, 7.8 mm x 30 cm, 10-micron and 13-micron, respectively) on an Agilent 1260 Infinity HPLC (Agilent Technologies, Inc.). Flow rate: 0.2 mL/min, 120-minute runtime per injection, 100 mcL injections. Mobile phase: 10% Sucrose, 20 mM HEPES, 0.05% Sodium Azide, pH 7.3. Column temperature = 35 ºC. UV detection @ 210, 280, 485 nm, with fluorescence detection at 485 nm excitation and 520 nm emission.

Disruptive Sandwich ELISA for GM-CSF Content

Virosome samples were disrupted by combining 20 mcL with 20 mcL 1% w/v Triton X-100 and sonicating for 5 x 1 second. Samples were diluted by adding 960 mcL PBS w/ 1% BSA and sonicated again for 5 x 1 second. Samples were further diluted in PBS w/ 1% BSA to reach a 500x final dilution. A GM-CSF standard curve was prepared, and the assay was conducted in accordance with manufacturer protocol (R & D Systems, Cat #MGM00). Briefly, 50 mcL of Assay Diluent was added to each well followed by 50 mcL of standard curve and sample dilutions. The plate was incubated at room temperature for 2 hours. The plate was then aspirated, washed 5x with wash buffer, and decanted. To each well, 100 mcL of murine GM-CSF Conjugate was added and the plate was incubated at room temperature for 2 hours. The plate was then aspirated, washed 5x

with wash buffer, and decanted. To each well, 100 mcL of substrate solution was added and the plate was incubated for 30 minutes at room temperature in the dark. The reaction was stopped with the addition of 100 mcL of Stop Solution to each well. The optical density was read at 450 nm and 570 nm (reference wavelength) on a Synergy H1 Plate Reader (BioTek Instruments, Inc.).

Disruptive Sandwich ELISA for ErbB2 Content

Virosome sample were disrupted by combining 20 mcL with 20 mcL 1% w/v Triton X-100 and sonicating for 5 x 1 second. The sample was then diluted by adding 960 mcL PBS w/ 1% BSA and sonicated again for 5 x 1 second. Samples were further diluted with PBS w/ 1% BSA to reach a 500x final dilution. An ErbB2 standard curve was prepared and the assay was conducted in accordance with manufacturer protocol, with the replacement of IC Diluent #12 and 14 with PBS w/ 1% BSA. Briefly, ErbB2 capture antibody was diluted to 4 mcg/mL in PBS and coated on a 96-well plate by incubating 100 mcL in each well overnight at room temperature. The plate was then aspirated, washed 5x with wash buffer, and decanted. The plate was blocked with 300 mcL PBS w/ 1% BSA at room temperature for 2 hours. The plate was then aspirated, washed 5x with wash buffer, and decanted. Standards and samples, 100 mcL each, were added and the plate was incubated at room temperature for 2 hours. The plate was then aspirated, washed 5x with wash buffer, and decanted. The detection antibody was diluted to 100 ng/mL in PBS w/ 1% BSA and 100 mcL was added to each well and incubated at room temperature for 2 hours. The plate was then aspirated, washed 5x with wash buffer, and

decanted. The streptavidin-HRP conjugate was diluted 1:200 and 100 mcL was added to each well and the plate was incubated in the dark at room temperature for 20 minutes. The plate was then aspirated, washed 5x with wash buffer, and decanted. Substrate solution was prepared and 100 mcL per well was added to the plate prior to incubation in the dark at room temperature for 20 minutes. The reaction was stopped through the addition of 50 mcL of Stop Solution and the optical density was read at 450 nm and 570 nm (reference wavelength) on a Synergy H1 Plate Reader (BioTek Instruments, Inc.).

MUNANA Assay for NA Activity

A 5-mg vial of 2′-(4-Methylumbelliferyl)-α-D-*N*-acetylneuraminic acid (MUNANA; see Supplemental Figure 26, for molecular structure) was dissolved in 1 mL PBS to reach ~100 mcM (Sigma Cat #M8639-5G, 489.41 Da, excitation 365 nm, emission 450 nm). A MUNANA working solution was prepared using a 10x dilution in PBS. Intact virosomes samples were diluted 50x by combining 20 mcL with 980 mcL PBS. The assay was conducted by combined 50 mcL of virosome 50x sample dilution and 100 mcL MUNANA working solution in a black 96-well plate. The plate was covered and incubated overnight (~19 hours) at 37 ºC and fluorescence was read with excitation at 365 nm and emission at 450 nm on a Synergy H1 Plate Reader (BioTek Instruments, Inc.).

SEC of Virosomes for NA Content

Intact virosome samples were diluted by combined 25 mcL with 100 mcL 10% Sucrose, 20 mM HEPES, pH 7.3 and 1 mcL anti-NA (H1N1) Antibody-FITC conjugate (Biorbyt Cat #orb188645). Samples were analyzed via SEC using G5000PWxl and G6000PWxl columns in series (Tosoh, Cat #08023 and 08024, 7.8 mm x 30 cm, 10-micron and 13-micron, respectively) on an Agilent 1260 Infinity HPLC (Agilent Technologies, Inc.). Flow rate: 0.2 mL/min, 120-minute runtime per injection, 100 mcL injections. Mobile phase: 10% Sucrose, 20 mM HEPES, 0.05% Sodium Azide, pH 7.3. Column temperature = 35 ^{o}C. UV detection @ 210, 280, 485 nm, with fluorescence detection at 490 nm excitation and 525 nm emission.

Disruptive Sandwich ELISA for Hemagglutinin Content

Virosome samples were disrupted by combining 20 mcL with 20 mcL 1% w/v Triton X-100 and sonicating for 5 x 1 second. Samples were diluted by adding 960 mcL PBS w/ 1% BSA and sonicated for 5 x 1 second. Samples were further diluted with Dilution Buffer to reach a 2500x final dilution. A HA standard curve was prepared, and the assay was conducted in accordance with manufacturer protocol (Sino Biological Cat #KIT11055). Briefly, capture antibody coated plates were washed 3x with wash buffer. The plate was then decanted. Standards and samples, 100 mcL each, were added and the plate was incubated at room temperature for 2 hours. The plate was then aspirated, washed 5x with wash buffer, and decanted. The detection antibody was diluted to 1

mcg/mL in Dilution Buffer and 100 mcL was added to the wells and incubated at room temperature for 1 hour. The plate was then aspirated, washed 5x with wash buffer, and decanted. Substrate Solution was prepared and 200 mcL was added to the plate and incubated in the dark at room temperature for 20 minutes. The reaction was stopped through the addition of 50 mcL Stop Solution and the optical density was read at 450 nm and 570 nm (reference wavelength) on a Synergy H1 Plate Reader (BioTek Instruments, Inc.).

Intact Sandwich ELISA for Hemagglutinin Content

Virosome samples were diluted 50x by combining 20 mcL with 980 mcL PBS w/ 1% BSA. The samples were further diluted with Dilution Buffer to reach a 2500x final dilution. A HA standard curve was prepared, and the assay was conducted in accordance with manufacturer protocol (Sino Biological Cat #KIT11055). Briefly, pre-coated capture antibody plates were washed 3x with wash buffer. The plate was then decanted. Standards and samples, 100 mcL each, were added and the plate was incubated at room temperature for 2 hours. The plate was then aspirated, washed 5x with wash buffer, and decanted. Detection antibody was diluted to 1 mcg/mL in Dilution Buffer and 100 mcL was added to wells and incubated at room temperature for 1 hour. The plate was then aspirated, washed 5x with wash buffer, and decanted. Substrate Solution was prepared and 200 mcL was added to the plate and incubated in the dark at room temperature for 20 minutes. The reaction was stopped through the addition of 50 mcL Stop Solution and the

optical density is read at 450 nm and 570 nm (reference wavelength) on a Synergy H1 Plate Reader (BioTek Instruments, Inc.).

Micro BCA Assay for Determination of Intact Virosome Total Protein Content

Virosome samples were diluted 25x by combining 20 mcL with 480 mcL PBS. A standard curve using Bovine Serum Albumin (BSA) was established by diluting 2 mg/mL stock to 200 mcg/mL and then conducting 2x serial dilutions thereafter using PBS. The assay was conducted in accordance with manufacturer recommended protocol (Thermo Scientific Cat #23235), using a BCA working solution of 25A:24B:1C. Standards and samples were plated using 100 mcL per well combined with 100 mcL of BCA working solution, the plate was covered and incubated at 37 ºC for 1.75 hours and the optical density was read at 562 nm on a Synergy H1 Plate Reader (BioTek Instruments, Inc.).

Statistical Analysis

Statistical analysis was conducted using Prism version 7.0c (GraphPad Software, Inc.). Differences between virosome and adjusome content groups were analyzed using Kruskal-Wallis test with Dunn's correction for multiple comparisons (multiplicity adjusted). Pre- and post-dialysis comparison of size and charge for adjusomes and virosomes stability were conducted using a 2-way ANOVA test with Sidak's correction. Adjusome and virosome size and charge stability differences were analyzed using a repeated measurement 2-way ANOVA test with Dunnett's correction for multiple

comparisons; all stability time-points were compared to the respective post-dialysis value. Comparative analysis of adjusome and virosome post-dialysis size and charge values was conducted using a Kruskal-Wallis test with Dunn's correction for multiple comparisons.

Chapter IV

Results

Virosomes were successfully produced and found to incorporate all components in DOPC and DOPG formulations, albeit some components were found to be in lesser quantities than expected. All virosomes were produced at 1 mL volume, were extruded, and 35 mcL was aliquoted for sizing and charge determination prior to dialysis. Some loss of material was observed during membrane extrusion due to extruder plunger leakage and occasional membrane blockage. The ErbB2, NA, and HA lyophilized protein vials were reconstituted using 10% Sucrose, 20 mM HEPES, pH 7.3, to reduce osmotic differences between virosome solutions and dialysis media. However, after 2 days of dialysis the virosome solutions were found to be approximately 700 mcL final volume. This reduction in volume is likely the result of osmotic gradients, due to the high concentration of sucrose used.

Though great care was taken during virosomal synthesis, production of nanoparticles at this scale is subject to variability due to small differences in processing, pipetting of small volumes or volatile organic solvents, and maintenance of a homogeneous solution. Additional propagation of error can be attributed to the assays employed and their respective variability. Potential translation of this technology would benefit from scaling of cost of goods and automation of production processes.

Evaluation of Adjusome Size and Charge

As an initial proof of concept screen, liposomes containing OxPAPC and MPLA (adjusomes) were produced in PBS and evaluated. The determination of adjusomes size indicated that the initial size of the adjusomes post-dialysis were in-line with expectations (~90-120 nm), with DOTAP liposomes of smaller diameter than DOPC and DOPG liposomes. However, upon storage at 2-8 ºC, DOTAP liposomes in PBS (137 mM sodium chloride, 10 mM sodium phosphate, pH 7.4) were observed to produce visible aggregates as depicted in Figure 2, suggesting a lack of stability.

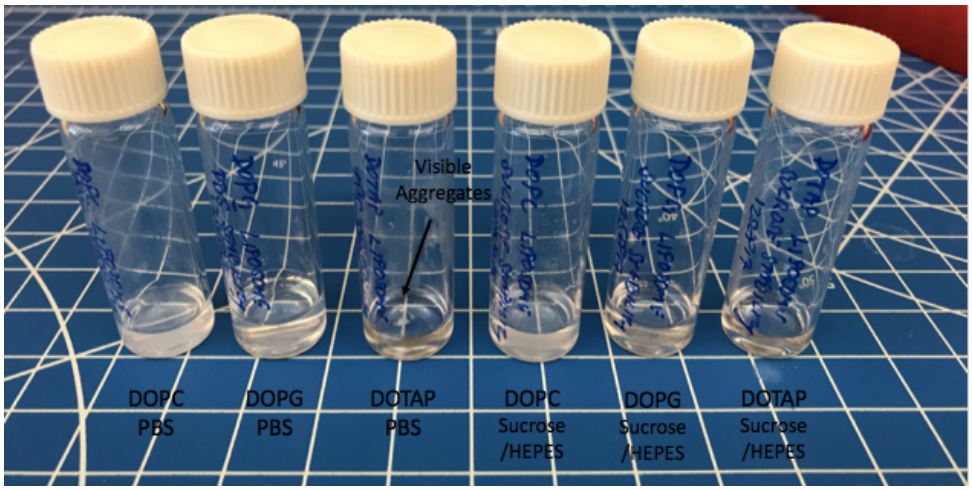

Figure 2. Photograph of liposome formulations after 7 days in PBS and Sucrose/HEPES reconstitution solutions. While most solutions were milky-white in appearance, the DOTAP formulation in PBS showed clear macroscopic aggregates (highlighted).

Due to this apparent lack of stability, liposomes and virosome products were reformulated using an isotonic 10% Sucrose, 20 mM HEPES, pH 7.3 reconstitution solution, based on commercial liposome formulations. A stability study was conducted to evaluate changes in nanoparticle size as a function of time. Results are summarized in

Figure 3, where DOPG and DOTAP liposomes rehydrated in PBS show a shift to greater diameters after dialysis. DOTAP liposomes displayed a statistically significant increase in size (> 500 nm) after dialysis, with major fluctuations in size likely due to sampling heterogeneity. In contrast, liposome formulations in 10% Sucrose, 20 mM HEPES, pH 7.3 show adequate stability through approximately 21 days. A trend of increasing size was observed for all formulations and a substantial increase in size was observed at 28 days for DOPC and DOPG formulations. However, differences were not statistically significant through 28 days of study. Representative light scattering profiles are given in Appendix 1, Supplemental Figures 1-12.

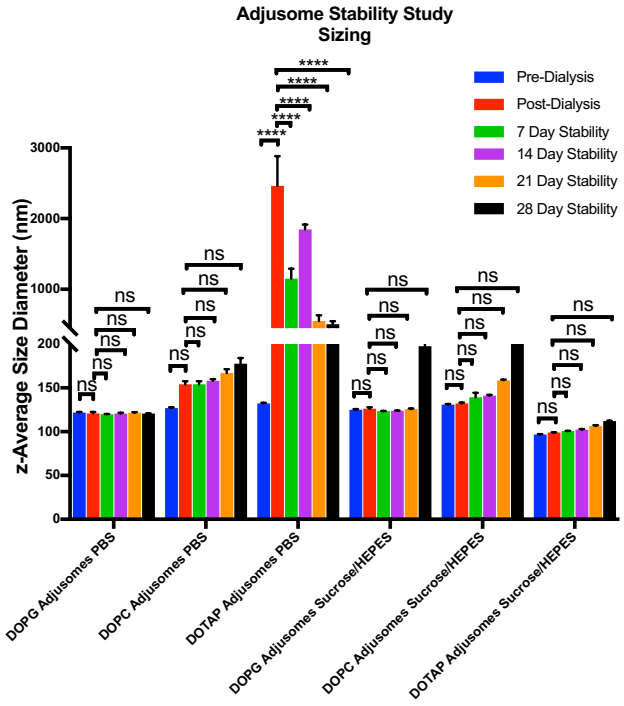

Figure 3. Summary of adjusome size stability in PBS and Sucrose/HEPES reconstitution solutions. Quantification of adjusome size as a function of time was evaluated across lipid formulations and reconstitution solutions – PBS versus 10% sucrose, 20 mM HEPES, pH 7.3. All solutions, with the exception of the DOTAP formulation in PBS, showed non-significant changes in size through 28 days of study. The DOTAP adjusomes displayed statistically significant changes in size after dialysis and at each time point thereafter. Values equal mean $\pm$ standard deviation (n=3 for each time point).

Adjusome charge was also evaluated on the PBS and Sucrose/HEPES rehydrated formulations and results obtained are consistent with expectations. The DOPG adjusomes are negatively charged, DOPC is closer to neutral – however negative due to the presence of a negative charge in MPLA – with DOTAP exhibiting a positive charge. Over time, DOPC and DOPG formulations in PBS were relatively consistent, reaching statistically significant differences intermittently through 28 days of study. The DOTAP formulation in PBS showed a shift to a more neutral zeta potential, reaching statistical significance consistently after 7 days. Evaluation of Sucrose/HEPES formulations suggest relatively stable charge distributions over time, however all formulations reached statistically significant differences after 14 days, see Figure 4 for a summary of results.

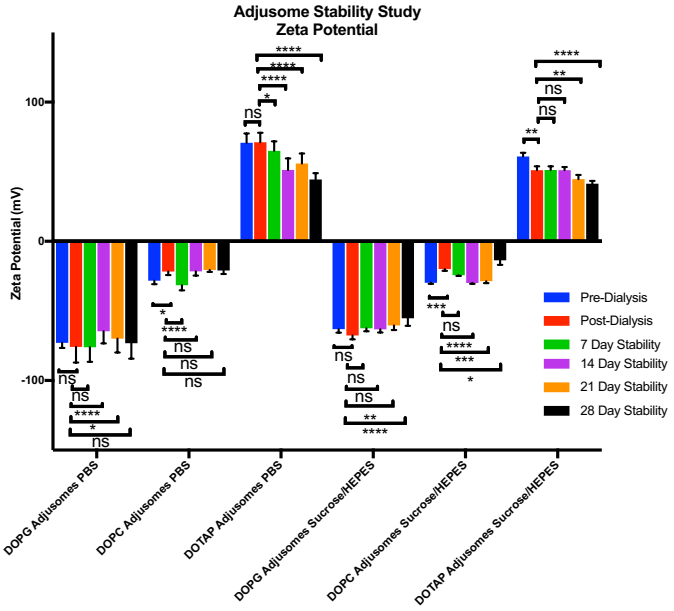

Figure 4. Summary of adjusome charge stability in PBS and Sucrose/HEPES reconstitution solutions. Quantification of adjusome charge as a function of time was evaluated across lipid formulations and reconstitution solutions – PBS versus 10% sucrose, 20 mM HEPES, pH 7.3. All solutions showed statistically significant changes in charge over time, however it is noted that the Sucrose/HEPES formulations are all non-significant through 7 days. Values equal mean $\pm$ standard deviation (n=3 for each time point). P-value: **** = $\leq$ 0.0001, *** = $\leq$0.001, ** = $\leq$0.01, * = $\leq$0.05, ns = not significant.

While this zeta potential data does reflect differences in particle charge, liposome stability is primarily evaluated through changes in particle size due to concerns regarding aggregation and coalescence. Aggregation, a reversible process, is the self-association of liposomes in solution, while coalescence is the fusion of liposomes to form larger particles, a non-reversible process (Yadav, 2011). Extensive aggregation can lead to precipitation of material out of solution, resulting in changes to product dose and quality. Both of these processes can lead to significant variations in cellular uptake (potency) and clearance through the RES system, while coalescence can lead to potential loss of encapsulated cargo.

Evaluation of Virosome Size and Charge

The determination of virosome size indicated that initial post-dialysis nanoparticle diameters were in line with expectations (~130-170 nm). Virosomes were observed to be of comparable (DOPC) or greater (DOPG and DOTAP) diameter than adjusomes, with DOTAP results being statistically significant as given in Figure 5. However, in contrast to adjusomes where the DOTAP formulation was smaller than both the DOPC and DOPG adjusomes, DOTAP virosomes were found to be significantly greater diameter than DOPC and DOPG counterparts.

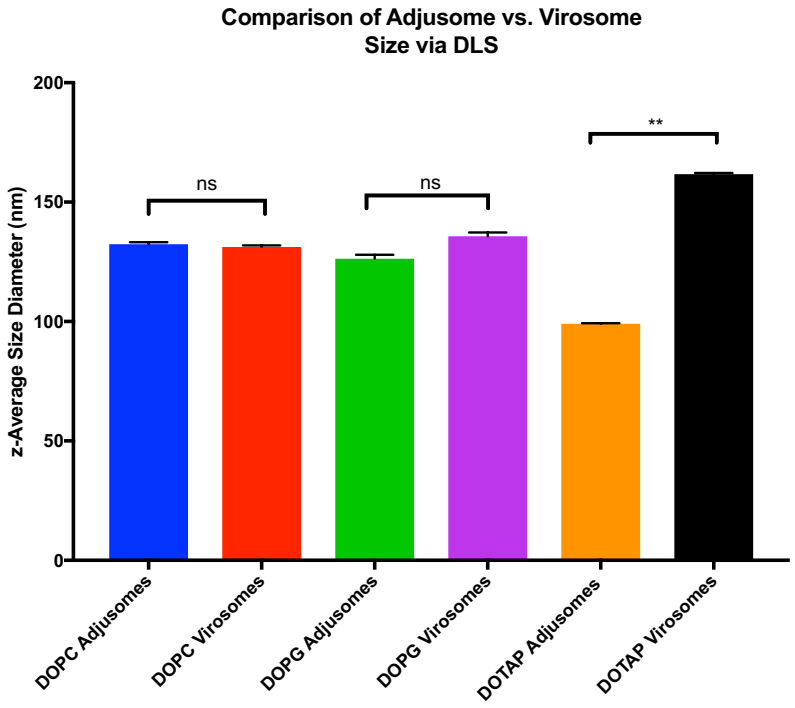

Figure 5. Comparison of adjusome and virosome size across lipid formulations. Quantitative comparison of adjusomes versus virosome size post-dialysis across lipid formulations in 10% sucrose, 20 mM HEPES, pH 7.3. Both DPOC and DOPG formulations were relatively comparable between adjusome and virosome products, while the DOTAP virosome was significantly greater in size. Values equal mean $\pm$ standard deviation (virosomes: n=9; liposome controls: n=3). P-value: ** = $\leq$ 0.01, ns = not significant.

A similar stability study was conducted on virosome lipid formulations in 10% sucrose, 20 mM HEPES, pH 7.3. Here, DOPC and DOPG virosome formulations showed adequate stability through 28 days of study, while DOTAP virosomes showed a progressive increase in size, these results are summarized in Figure 6. DOTAP virosomes showed a statistically significant increase in size after 7 days, reaching ~300 nm diameter and ~1120 nm through 28 days. Though a shift in size and polydispersity was found at day 7 and 28, no visible aggregation was observed, see Figures 7 and 8. Although some increase in size was observed as a function of time, the resulting DOPC and DOPG virosome diameters are still within size expectations and should not be expected to result

in significant loss of nanoparticle activity. In comparison, DOTAP virosomes were found to be relatively unstable in sucrose/HEPES solution, suggesting that they would require use immediately after preparation; the effect of this size difference could lead to leakage of cargo and potential loss of activity if this change in size is the result of coalescence.

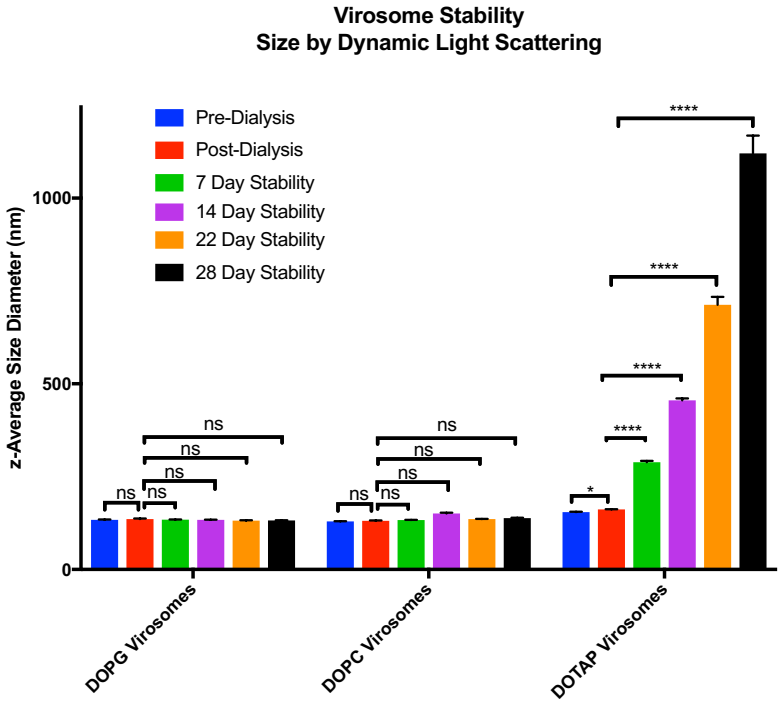

Figure 6. Summary of virosome size stability in Sucrose/HEPES reconstitution solution. Quantification of virosome size as a function of processing/time across lipid formulations in 10% sucrose, 20 mM HEPES, pH 7.3. DOPC and DOPG virosomes were observed to show non-significant changes in size over 28 days of study, while the DOTAP formulation displays significant changes after dialysis and at subsequent time point thereafter. Values equal mean $\pm$ standard deviation (n=3 for each time point). P-value: **** = $\leq$ 0.0001, * = $\leq$0.05, ns = not significant.

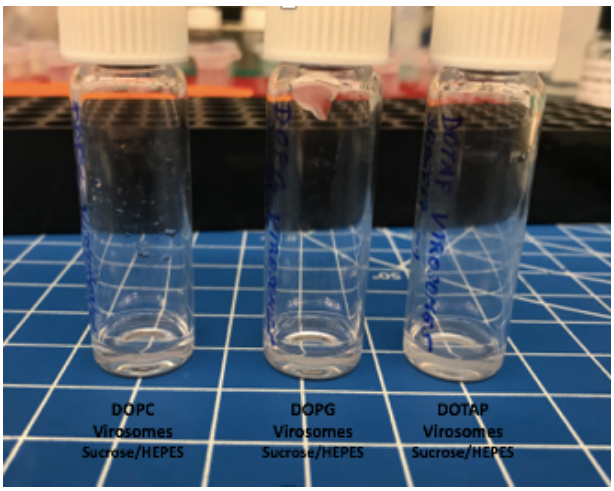

Figure 7. Photograph of virosome formulations after 7 days in Sucrose/HEPES reconstitution solution. Left: DOPC, center: DOPG, and right: DOTAP. All preparations were rehydrated with 10% sucrose, 20 mM HEPES, pH 7.3 and were milky-white in appearance, with no appearance of macroscopic aggregation.

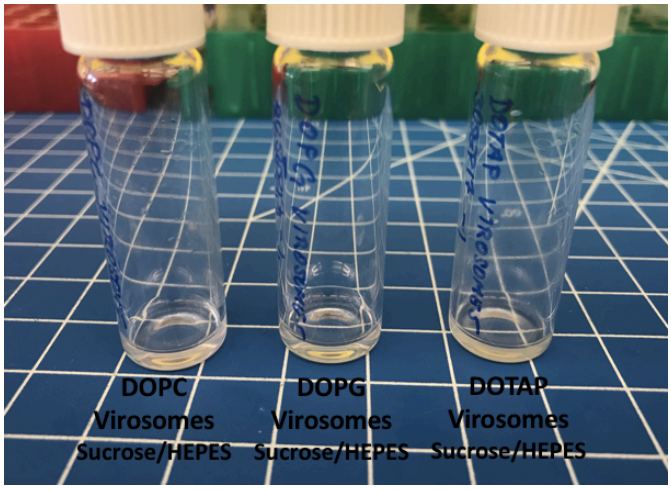

Figure 8. Photograph of virosome formulations after 28 days in Sucrose/HEPES reconstitution solution. Left: DOPC, center: DOPG, and right: DOTAP. All preparations were rehydrated with 10% sucrose, 20 mM HEPES, pH 7.3 and were milky-white in appearance, with no appearance of macroscopic aggregation.

These same virosome samples were also assayed for the determination of charge, where a shift in zeta potential was observed when compared to the corresponding adjusomes. In all formulations a shift was observed, with DOPG and DOTAP virosomes

shifting towards a more neutral charge and DOPC shifting more negatively. No changes in zeta potential were statically significant, these results are summarized in Figure 9.

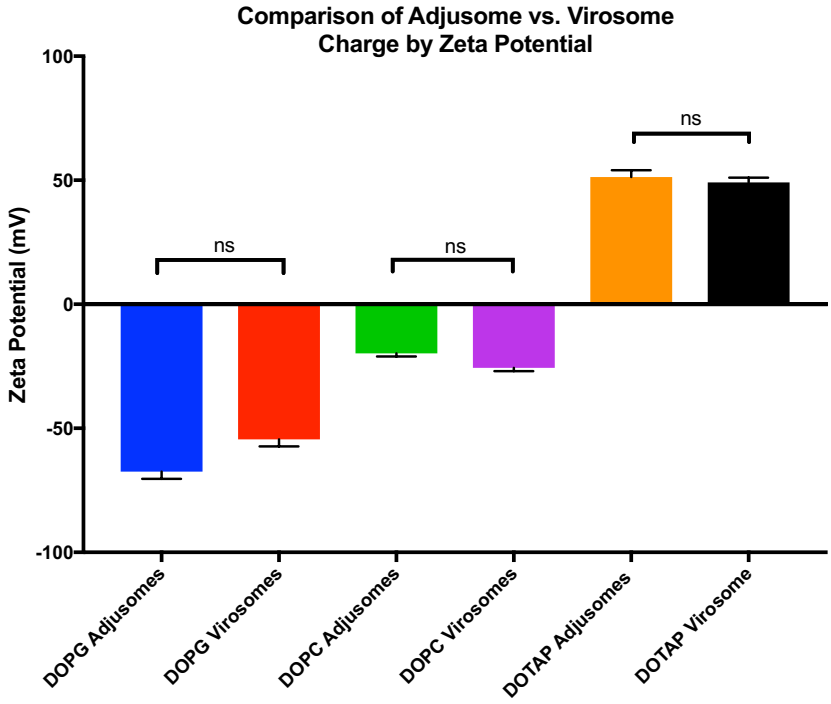

Figure 9. Comparison of liposome and virosome charge across lipid formulations. Quantification of adjusomes versus virosome charge post-dialysis across lipid formulations in 10% sucrose, 20 mM HEPES, pH 7.3. No statistically significant difference was found between adjusomes and virosomes across all lipid formulations. Values equal mean $\pm$ standard deviation (n=3). P-value: ns = not significant.

The analysis of virosome charge was extended into a stability study, where both DOPG and DOTAP virosome formulations exhibited a statistically significant time dependent trend in charge towards neutrality. In contrast, DOPC virosomes appeared relatively stable through 28 days of testing, only exhibiting an intermittent statistical significance at 7 days, these results are summarized in Figure 10.

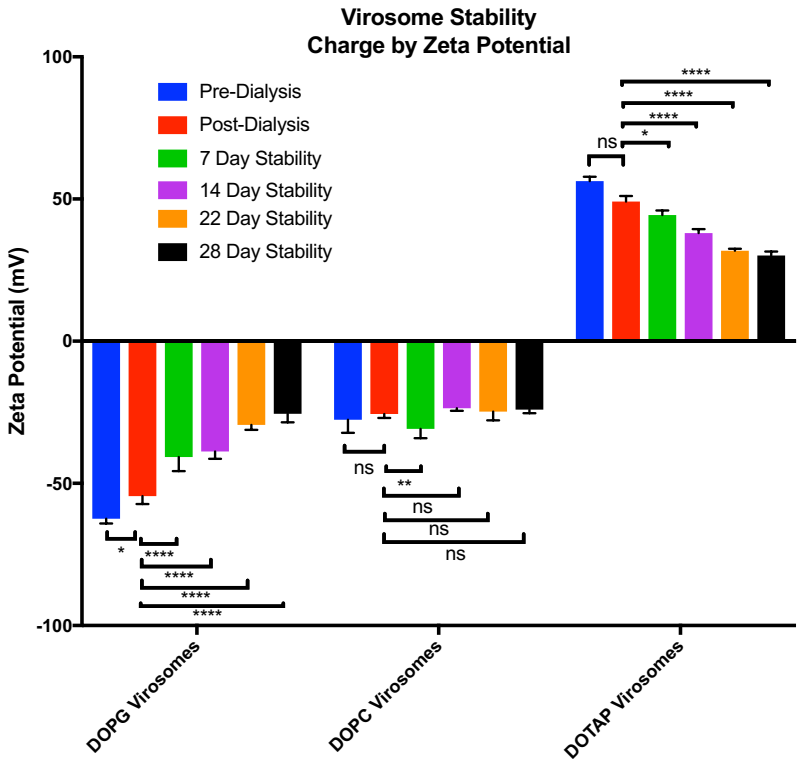

Figure 10. Summary of virosome charge stability in Sucrose/HEPES reconstitution solution. Quantification of liposome charge as a function of time across lipid formulations in 10% sucrose, 20 mM HEPES, pH 7.3. DOPC virosomes display relative stability, while DOPG and DOTAP formulations show a statistically significant progression toward charge neutrality over time. Values equal mean ± standard deviation (n=3 for each time point). P-value: **** = ≤ 0.0001, ** = ≤0.01, * = ≤0.05, ns = not significant.

The initial virosome production – pre- and post-dialysis – size, polydispersity index, and charge results for the three lipid formulations are summarized in Tables 1-3.

Table 1. Summary of DOPC virosome Zetasizer results.

DOPC Virosomes	z-Average Diameter (nm)	PDI	Zeta Potential (mV)
Pre-Dialysis	130.7 ± 3.8	0.099 ± 0.013	-25.8 ± 3.1
Post-Dialysis	134.4 ± 4.3	0.087 ± 0.018	-21.6 ± 3.2

Summary of DOPC virosome size, PDI, and charge characteristics as a function of dialysis processing.

Table 2. Summary of DOPG virosome Zetasizer results.

DOPG Virosomes	z-Average Diameter (nm)	PDI	Zeta Potential (mV)
Pre-Dialysis	133.4 ± 4.0	0.078± 0.015	-62.7 ± 2.9
Post-Dialysis	135.8 ± 3.6	0.071 ± 0.024	-59.8 ± 4.7

Summary of DOPG virosome size, PDI, and charge characteristics as a function of dialysis processing.

Table 3. Summary of DOTAP virosome Zetasizer results.

DOTAP Virosomes	z-Average Diameter (nm)	PDI	Zeta Potential (mV)
Pre-Dialysis	155.3 ± 4.1	0.109 ± 0.013	56.8 ± 2.7
Post-Dialysis	167.3 ± 5.2	0.115 ± 0.018	50.5 ± 2.1

Summary of DOTAP virosome size, PDI, and charge characteristics as a function of dialysis processing.

The polydispersity across all three formulations are comparable and show a relatively tight size distribution, with minimal difference observed through dialysis.

Further, sizing profiles for these virosomes - pre- and post-dialysis and through 7-day stability - are provided in Appendix 3, Supplemental Figures 13-21.

Evaluation of MPLA Content in Virosomes

The ability to incorporate the potent adjuvant MPLA, a less toxic synthetic version of lipopolysaccharide (LPS), into a virosomal lipid bilayer was evaluated. Endotoxin free water and reagents were used in virosome production processing in order to isolate the response from MPLA, as the phospholipid is the only component capable of stimulating a LAL response in these virosomes. The MPLA content was determined using an EndoSafe LAL cartridge kit after disruption of samples via Triton X-100 and sonication treatment. Results indicated that MPLA content was differential across lipid formulations with the greatest content found in DOPG formulations, followed by DOPC virosomes. DOTAP virosomes did not appear to contain any significant MPLA, see Figure 11 for a summary of results. Both DOPC and DOPG content values were statistically significant when compared to the DOTAP content. Analysis of liposome control samples (Cholesterol + DOPC/DOPG/DOTAP), showed moderate signal from DOPG liposomes, with minimal endotoxin found in DOPC and DOTAP liposomes. DOTAP liposome control samples interfered with assay controls across dilutions and were consistently below the limit of quantification (LOQ), therefore LOQ values are reported.

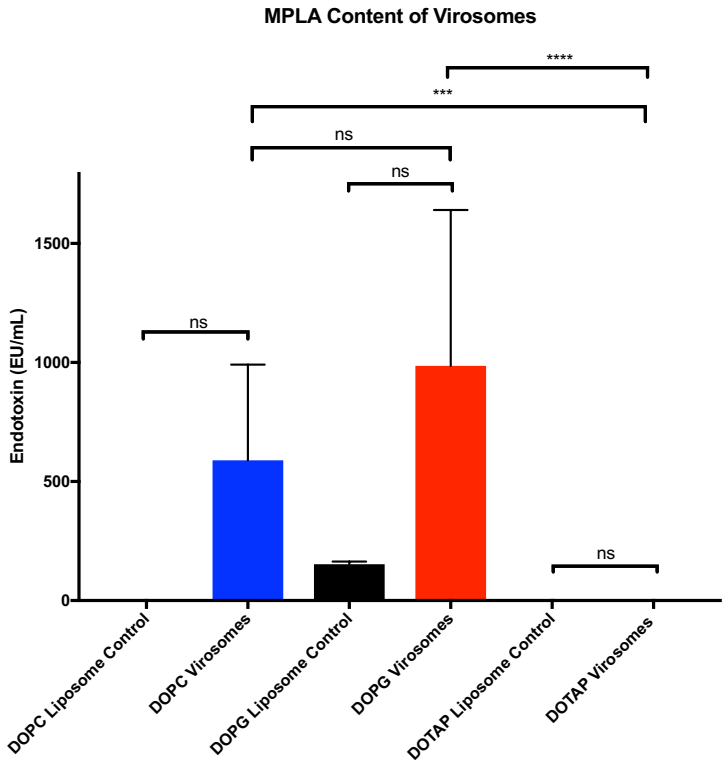

Figure 11. Summary of MPLA content of disrupted virosomes across lipid formulations. Quantification of MPLA content across lipid formulations as determined by the EndoSafe assay. The adjuvant MPLA was found to be readily incorporated in both DOPC and DOPG virosomes formulations, with minimal content observed in the DOTAP formulation. Values equal mean $\pm$ standard deviation (virosomes: n=9; liposome controls: n=3). P-value: **** = $\leq$ 0.0001, *** = $\leq$0.001, ns = not significant.

The concentrations obtained are less than expected, approximately 0.5 mcg/mL (DOPC) and 1 mcg/mL (DOPG), however these values are well within efficacious concentrations for the stimulation of TLR4 (10 ng – 10 mcg/mL). It is noted that the DOPG liposome control (DOPC + Cholesterol) showed high endotoxin values, suggesting that this lipid formulation interferes with the assay.

Determination of OxPAPC Content

The ability to incorporate the lipid DAMP – OxPAPC – into the external surface of virosomes was evaluated using two orthogonal analytical methods. The OxPAPC content of virosomes was evaluated using a sandwich ELISA where intact virosomes were captured using an anti-HA ELISA kit and subsequently analyzed using an anti-OxPAPC E06 antibody. Results, as summarized in Figure 12, indicated that OxPAPC was incorporated comparably across DOPC and DOPG lipid formulations, with minimal incorporation into DOTAP virosomes. Both DOPC and DOPG content values were statistically significant when compared to the DOTAP content. Given the low concentration of OxPAPC observed in samples, this assay required significant assay development to acquire adequate signal. To resolve this, the Streptavidin-HRP conjugate concentration was increased to further amplify signal. Given the lack of corresponding OxPAPC virosomal standards, results are presented as relative absorbance. Further, as this assay utilizes intact virosomes, results given demonstrate that OxPAPC is externally presented on the lipid bilayer, analogous to presentation of the DAMP on the cell surface after damage. Analysis of control liposomes (cholesterol + DOPC/DOPG/DOTAP) suggest minimal virosome-antibody non-specific interaction.

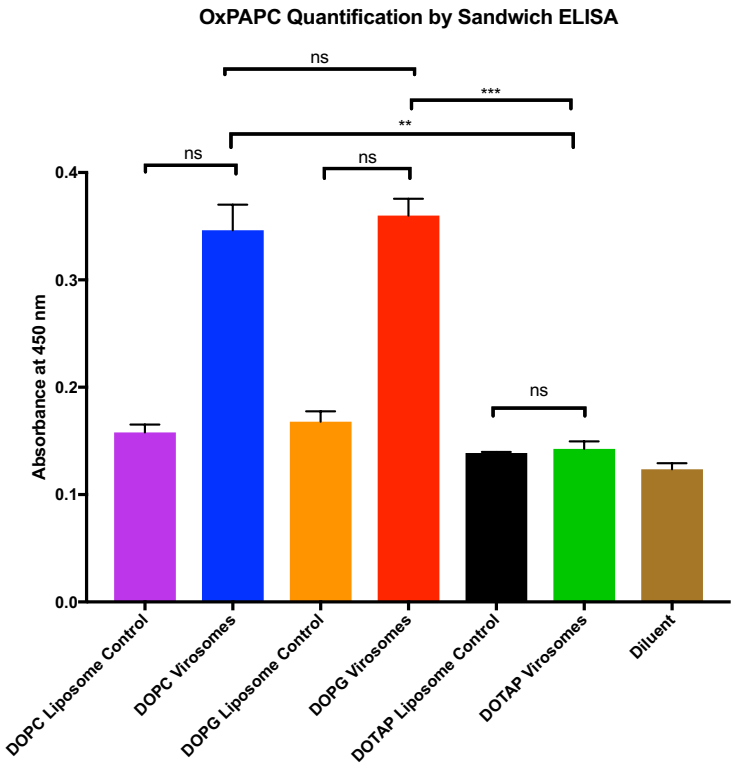

Figure 12. Summary of OxPAPC content of intact virosomes as determined by sandwich ELISA. Quantification of OxPAPC incorporation across lipid formulations as determined by sandwich ELISA. The adjuvant OxPAPC was observed to be incorporated into DOPC and DOPG virosomes, with minimal content found in DOTAP virosomes. Values equal mean $\pm$ standard deviation (virosomes: n=9; liposome controls: n=3). P-value: *** = $\leq$ 0.001 ** = $\leq$ 0.01, ns = not significant.

The OxPAPC content of virosomes was also determined by size exclusion chromatography (SEC) after incubation with the anti-OxPAPC E06 antibody. As analysis was conducted on intact virosomes, binding of the antibody quantitates OxPAPC displayed on the exterior of the lipid bilayer. Quantification by this method resulted in a strong interaction with the DOPG lipid complex. In contrast, moderate signal was obtained from DOPC virosome, with minimal non-specific ionic interaction with the DOPC liposome. No signal was obtained from either liposome control or virosome DOTAP formulations. However, it is noted that the DOTAP formulation had reduced free antibody signal – both fluorescence and UV – suggesting that this method may not be

compatible with DOTAP lipids. Although a fluorescent antibody was used here, greater signal to noise was obtained at 280 nm absorbance, therefore these results are reported here as given in Figure 13. The content differences between DOPG and DOTAP virosomes were found to be statistically significant. Analysis of control liposomes (cholesterol + DOPC/DOPG/DOTAP) suggest a strong secondary ionic interaction between DOPG liposome formulations and the antibody, with minimal interaction across the DOPC and DOTAP formulations.

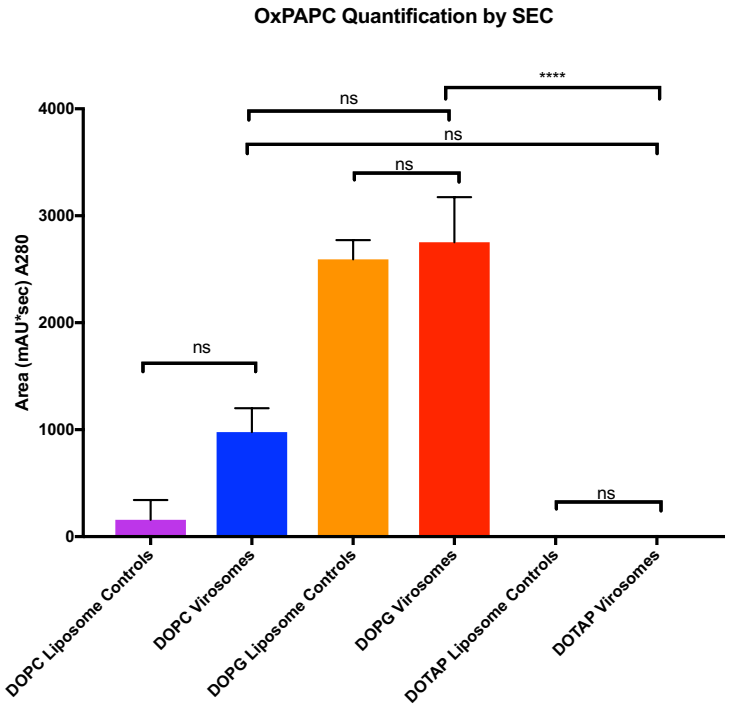

Figure 13. Summary of OxPAPC content of intact virosomes as determined by SEC. Quantification (A280) of OxPAPC display on virosomes across virosome formulations showed no statistical difference from corresponding controls. Values equal mean $\pm$ standard deviation (virosomes: n=9; liposome controls: n=3). P-value: **** = $\leq$ 0.0001, ns = not significant.

Representative chromatograms for both virosome samples and liposome controls are provided in Figures 14 and 15.

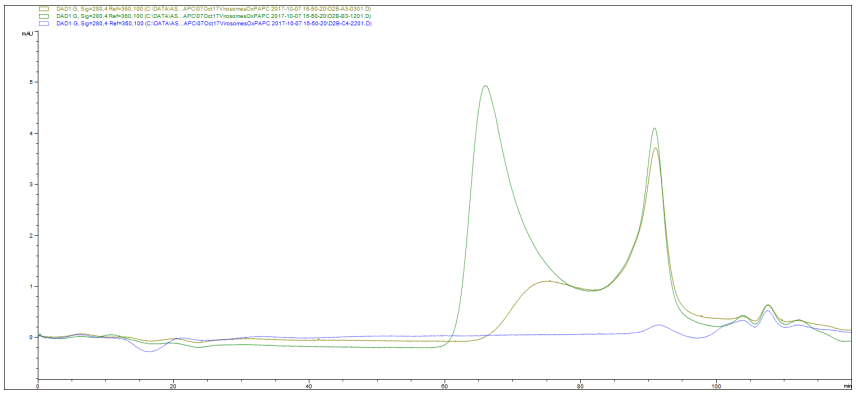

Figure 14. Representative overlay of SEC chromatograms of virosome OxPAPC content across lipid formulations. Chromatograms (absorbance at 280 nm) show evident retention time shift between free antibody and virosome-antibody complex for DOPC and DOPG formulations, minimal signal is observed for DOTAP virosomes or related free antibody. Orange: DOPC Virosomes; Green: DOPG virosomes; Blue: DOTAP virosomes. Virosome-antibody complex is observed at approximately 70 min, with free antibody eluting at approximately 90 min.

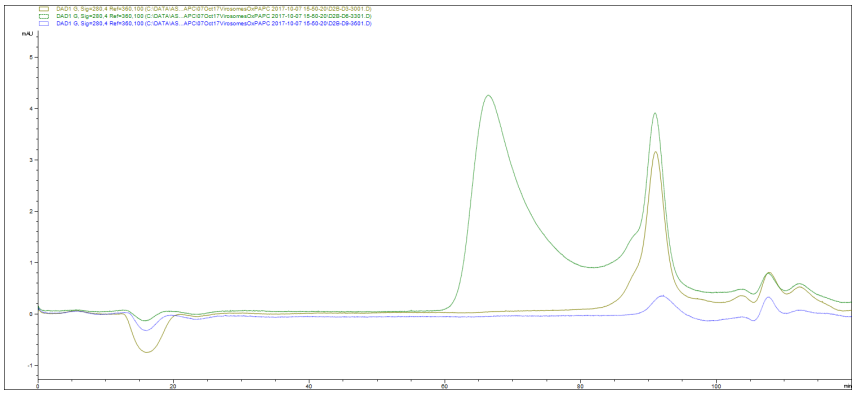

Figure 15. Representative overlay of SEC chromatograms of liposome control OxPAPC content across lipid formulations. Chromatograms (absorbance at 280 nm) show retention time shift between free antibody and adjusome-antibody complex for the DOPG liposome, minimal signal is observed for DOPC and DOTAP formulations. Orange: DOPC liposomes; Green: DOPG liposomes; Blue: DOTAP liposomes. Liposome-antibody complex is observed at approximately 70 min, with free antibody eluting at approximately 90 min.

Sandwich ELISA for GM-CSF Content

The quantification of virosome associated GM-CSF, the dendritic cell recruiting and stimulating cytokine, was evaluated using an ELISA assay after lipid disruption using Triton X-100 and sonication treatment. Results, as depicted in Figure 16, indicate that there is a significant encapsulation into DOPG virosomes, with moderate incorporation into the DOPC formulation and minimal GM-CSF in DOTAP virosomes. The content values of DOPG virosomes were found to be statistically significant when compared to those of DOTAP virosomes. Adjusome controls (Cholesterol + OxPAPC + MPLA + DOPC/DOPG/DOTAP) did not display any appreciable signal.

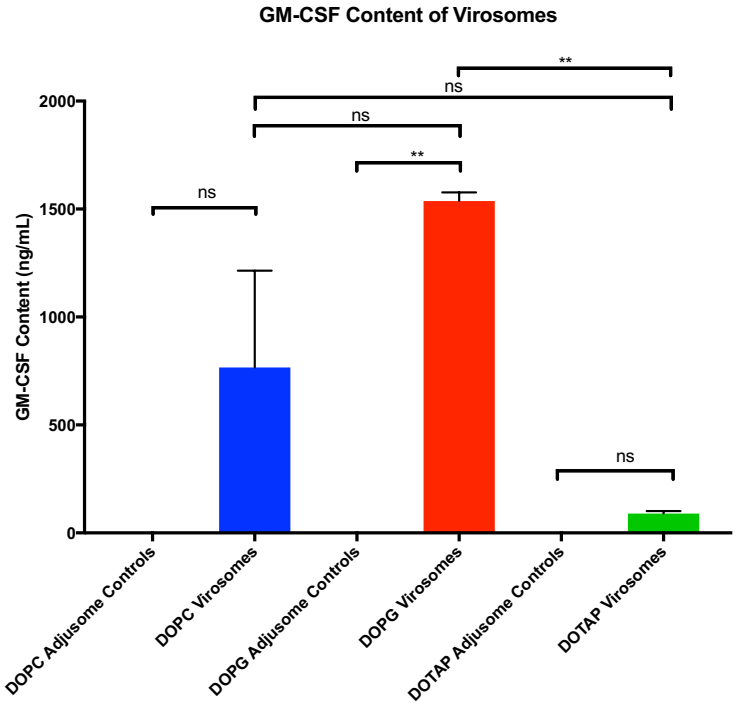

Figure 16. Summary of GM-CSF content of virosomes as determined by disruptive sandwich ELISA. Quantification of DOPC and DOPG virosomes are found to contain appreciable levels of GM-CSF, while DOTAP virosomes are observed to contain minimal quantities. Values equal mean $\pm$ standard deviation (virosomes: n=9; liposome controls: n=3). P-value: ** = $\leq$0.01, ns = not significant.

It is noted that the concentrations obtained for the DOPG formulation are in line with efficacious dose determined by Ali, et. al. (~1-3 mcg) and reached encapsulation efficiencies of ~8%. However, this assay is incapable of distinguishing between encapsulated and lipid-associated extra-virosomal GM-CSF, the latter is assumed to be a minimal contribution due to the extent of dialysis. As suggested in the introduction, bolus administration of GM-CSF may be required in order to recruit dendritic cells to the local administration site, however this data suggests that GM-CSF can be readily incorporated into these virosomes with modest efficiency.

Sandwich ELISA for ErbB2Content

The determination of ErbB2 content of virosomal formulations was evaluated using an ErbB2 specific sandwich ELISA after virosomal disruption using Triton X-100 and sonication treatment. Results, as presented in Figure 17, indicate that the ErbB2 antigen is well incorporated into all three virosome formulations, with greatest incorporation found in DOPC virosomes, followed by DOPG and then DOTAP formulations. There was no statistical difference between virosome formulations when compared to each other. Adjusome controls (Cholesterol + OxPAPC + MPLA + DOPC/DOPG/DOTAP) did not display any significant signal. In contrast to the relatively low incorporation efficiency of GM-CSF, the ErbB2 protein incorporation reached ~12-17%. However, here again the assay is incapable of distinguishing between encapsulated and lipid membrane associated ErbB2 protein. In biologically active virosomes,

encapsulated ErbB2 protein should be processed and presented though the MCH I pathway as previously discussed.

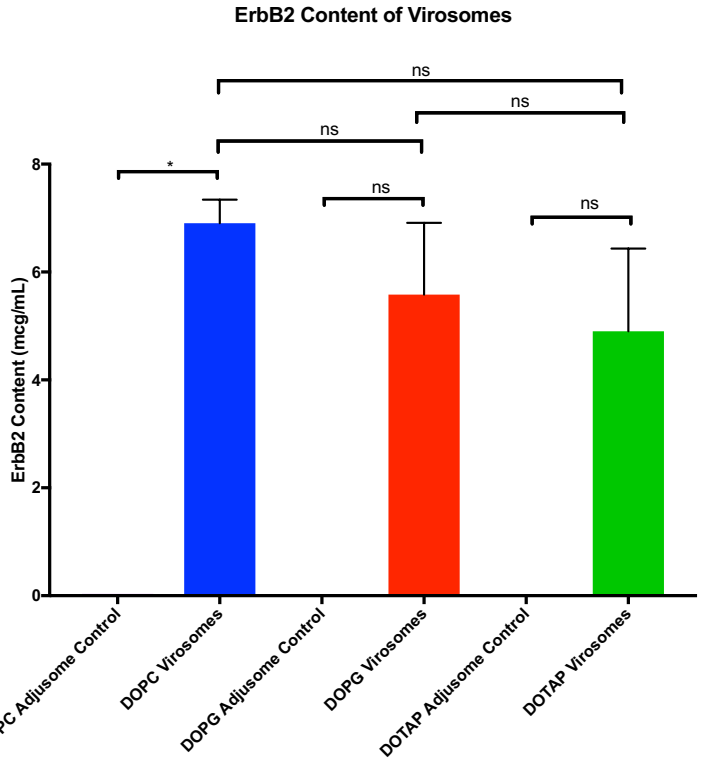

Figure 17. Summary of ErbB2 content of disrupted virosomes as determined by sandwich ELISA. Quantification of the antigen ErbB2 incorporation was comparable across all virosome lipid formulations. Values equal mean $\pm$ standard deviation (virosomes: n=9; liposome controls: n=3). P-value: * = $\leq$0.05, ns = not significant.

Determination of NA Content

The ability to incorporate and display neuraminidase (NA) was evaluated using two orthogonal analytical methods – SEC and an intact virosomal NA activity assay – both of which indicted that NA was successfully displayed on the exterior of the virosomes. The virosomal content of neuraminidase was determined using a carbohydrate-fluorophore conjugate to which NA possesses hydrolytic enzymatic

activity. In the presence of NA, the substrate 2′-(4-Methylumbelliferyl)-α-D-*N*-acetylneuraminic acid (MUNANA, see Supplemental Figure 26) is readily cleaved. The fluorescent product was detected with excitation at 365 nm and emission at 450 nm after overnight incubation at 37 ºC. Results indicate that DOPC and DOPG virosomes have significant activity, while DOTAP virosomes displayed background hydrolysis. Both DOPC and DOPG virosome activity was statistically significant when compared to the DOTAP formulation. Temporally dependent hydrolysis of the substrate was observed in media only and NA-free adjusome controls (Cholesterol + OxPAPC + MPLA + DOPC/DOPG/DOTAP), however results are comparable suggesting a background hydrolysis rate, see Figure 18. Further, as intact virosomes were incubated with MUNANA substrate, this assay simultaneously establishes extra-virosomal display of NA as well as the presence of conformational active NA protein. Due to the lack of a comparable NA standard, for both methods, results are presented as relative values across lipid formulations.

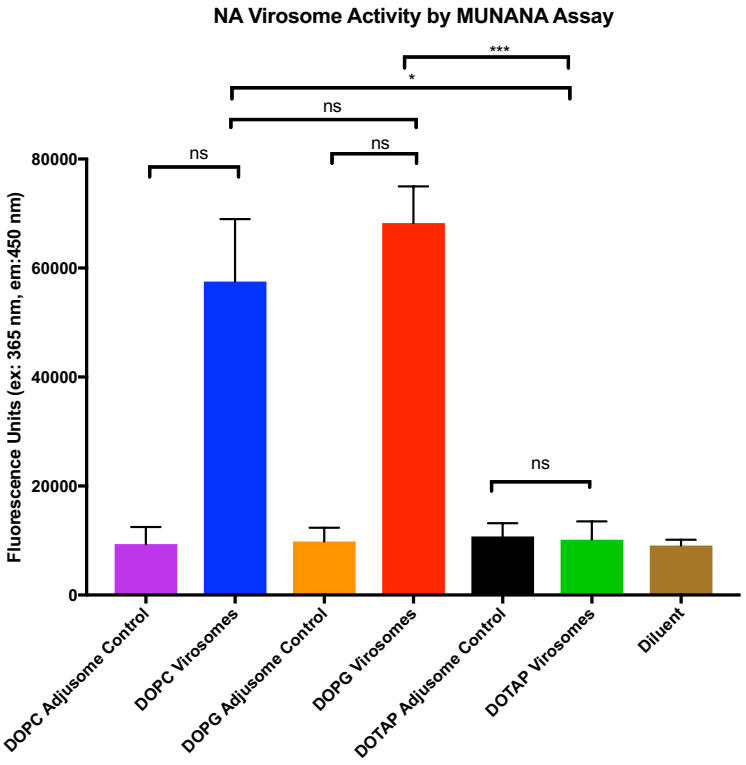

Figure 18. Summary of NA content of intact virosomes as determined by MUNANA assay. Both DOPC and DOPG virosomes displayed NA enzymatic activity, while DOTAP virosome activity was comparable to background. Values equal mean ± standard deviation (virosomes: n=9; liposome controls: n=3). P-value: *** = ≤0.001, * = ≤0.05, ns = not significant.

The NA content of virosomes was also determined by size exclusion chromatography after incubation with anti-NA-FITC antibody. Quantification by this method resulted in a significant shift in peak retention time for the DOPG virosomes, with minimal signal from DOPC, and no significant signal obtained from DOTAP formulations. The content difference between DOPG and DOTAP virosomes was found to be statistically significant. It is noted that the DOTAP formulation had reduced free antibody signal – both fluorescence and UV – suggesting that this method may not be compatible with DOTAP lipids. Although a fluorescent antibody was in this analysis, greater signal to noise was obtained at 280 nm absorbance, therefore these results are

reported here. Analysis of control adjusomes (cholesterol + OxPAPC + MPLA + DOPC/DOPG/DOTAP) suggest a very strong secondary interaction between DOPG liposome formulations and the antibody, and minimal interaction across the DOPC and DOTAP formulations. Results are summarized in Figure 19, with representative chromatograms for virosomes and liposome controls, presented in Figures 20 and 21.

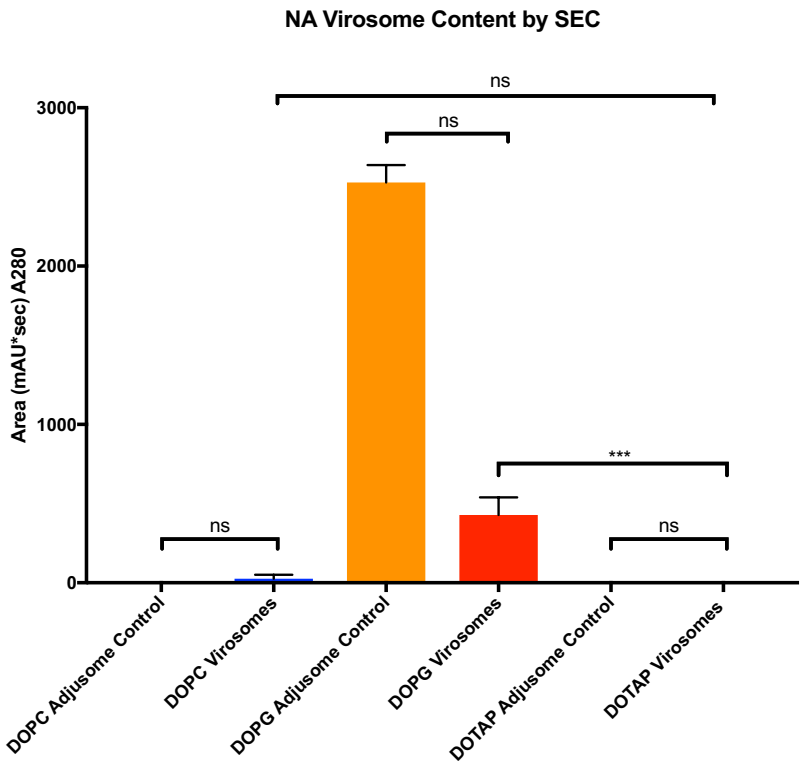

Figure 19. Summary of NA content of intact virosomes as determined by SEC. Quantification (absorbance at 280 nm) of NA display on virosomes across virosome formulations revealed minor signal across all virosomes, the difference between DOPG and DOTAP formulations was found to be significant. A strong antibody-DOPG adjusome control interaction was noted. Values equal mean $\pm$ standard deviation (virosomes: n=9; liposome controls: n=3). P-value: *** = $\leq$0.001, ns = not significant.

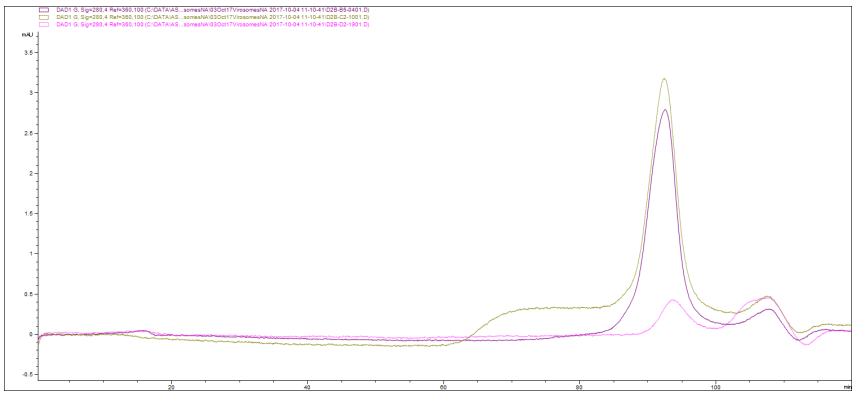

Figure 20. Representative overlay of SEC chromatograms of virosome NA content across lipid formulations. Chromatograms (absorbance at 280 nm) show evident retention time shift between free antibody and virosome-antibody complex the DOPG formulation, minimal signal is observed for DOPC and DOTAP virosomes or related free antibody. Purple: DOPC Virosomes; Orange: DOPG virosomes; Pink: DOTAP virosomes. Virosome-antibody complex is observed at approximately 70 min, with free antibody eluting at approximately 90 min.

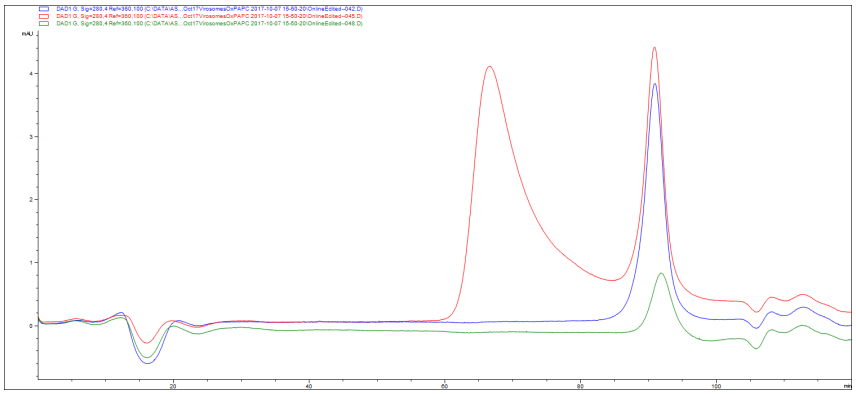

Figure 21. Representative overlay of SEC chromatograms of liposome control NA content across lipid formulations. Chromatograms (absorbance at 280 nm) show evident retention time shift between free antibody and liposome-antibody complex for the DOPG formulations, minimal signal is observed for DOPC and DOTAP liposomes or related free antibody. Blue: DOPC liposomes; Red: DOPG liposomes; Green: DOTAP liposomes. Liposome-antibody complex is observed at approximately 70 min, with free antibody eluting at approximately 90 min.

While size exclusion chromatography analysis was expected to facilitate the quantification of OxPAPC and NA on intact virosomes, it was recognized that DOTAP formulations of virosomes showed no nanoparticle related shift in retention and a reduced detection antibody signal. The reason for this is not clear as SEC columns (Tosoh, Inc.)

are comprised of a hydroxylated polymethacrylate and therefore should not be anticipated to result in ionic interactions. However, it was anecdotally noted that after sequential DOTAP virosomal injections, the back pressure of the columns was substantially higher suggesting that nanoparticles were accumulating at the column head. Subsequent column cleaning using 20% acetonitrile – capable of dissolution of lipid nanoparticles – was found to alleviate this back pressure. Columns were cleaned in between OxPAPC and NA SEC analyses, given this observation.

Determination of HA content

The incorporation of hemagglutinin (HA) was evaluated using two analytical methods, intact and disruptive virosome sandwich ELISA assays. An intact virosome sandwich ELISA was developed where whole virosomes were captured using an anti-HA ELISA kit. Results indicate that HA is incorporated across DOPC and DOPG lipid formulations, with greater incorporation into DOTAP virosomes, see Figure 22. The HA content of DOPG and DOTAP virosomes was found to be the only statistically significant difference. Further, as this assay utilizes intact virosomes, results given demonstrate that HA is presented outside of the lipid bilayer. Analysis of control adjusomes (Cholesterol + OxPAPC + MPLA + DOPC/DOPG/DOTAP) suggest minimal non-specific virosome-antibody interaction.

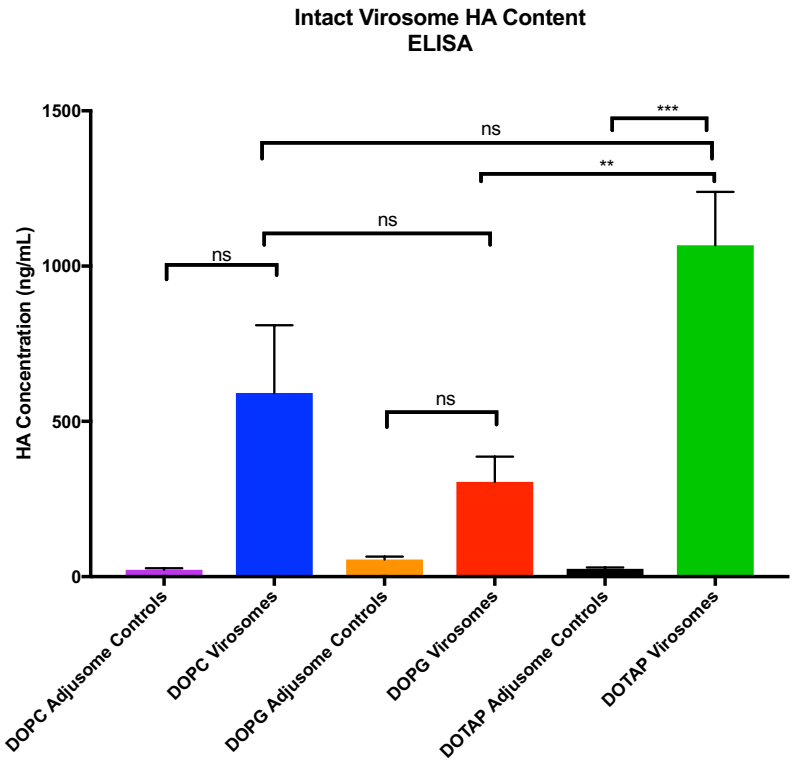

Figure 22. Summary of HA content of intact virosomes as determined by sandwich ELISA. Quantification of HA display on virosomes shows incorporation across all lipid formulations with greatest content found in DOTAP virosomes. Values equal mean $\pm$ standard deviation (virosomes: n=9; liposome controls: n=3). P-value: *** = $\leq$0.001, ** = $\leq$0.01, ns = not significant.

The Hemagglutinin content was also evaluated via a HA ELISA kit after disruption of virosomes via Triton X-100 and sonication treatment. Using this disruption method, both membrane associated and encapsulated HA should become soluble and therefore accessible for quantification via ELISA. Similar to the intact HA virosome, results indicate a strong incorporation into DOTAP lipid formulations, with reduced incorporation into DOPG and minimal incorporation into DOPC virosomes. No statistically significant difference was found across virosome formulations. Analysis of control intact adjusomes (Cholesterol + OxPAPC + MPLA + DOPC/DOPG/DOTAP)

suggest minimal non-specific virosome-antibody interaction. Results are summarized in Figure 23.

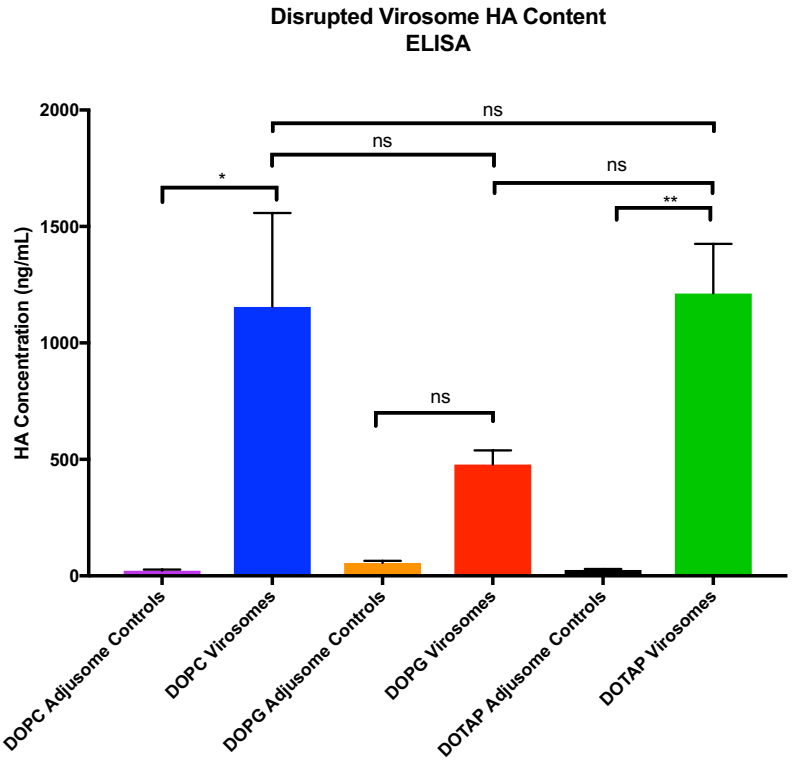

Figure 23. Summary of HA content of disrupted virosomes as determined by sandwich ELISA. Quantification of total virosomal HA content reveals incorporation in all virosomes with no statistical difference between lipid formulations. Values equal mean $\pm$ standard deviation (virosomes: n=9; liposome controls: n=3). P-value: ** = $\leq$0.01, * = $\leq$0.05, ns = not significant.

The quantitation conducted using intact virosomes was similar (~50-90%) of that obtained using the disruptive approach suggesting that the majority of incorporated HA is found on the exterior of the virosome complex. Based on intact virosome HA content, incorporation efficiencies were between ~2.5-5% across lipid formulations.

Determination of Extra-Virosomal Total Protein

As an orthogonal method to determine protein displayed on the exterior of the virosome a bicinchoninic acid (BCA) assay was employed. The assay is a nonspecific titration of total protein in solution, where colorimetric development is proportional to the amount of protein amide bonds present. Although samples were quantitated against a BSA standard, only relative concentrations should be evaluated here due to differences in assay performance across proteins and potential interference from the relatively high lipid content (Olson, 2007). Results indicate the presence of significant protein content in DOPC and DOPG virosomal formulations, and minimal protein content in DOTAP virosomes. Both DOPC and DOPG virosomes were found to be statistically significant when compared to the DOTAP formulation. Analysis of control intact adjusomes (Cholesterol + OxPAPC + MPLA + DOPC/DOPG/DOTAP) suggest minimal non-specific reaction with the BCA reagent, see Figure 24 for a summary of results. These results parallel those obtained for NA by the MUNANA activity assay suggesting that that majority of protein found on the exterior of the DOPC and DOPG virosomes is NA, which is consistent with the relatively low HA incorporation efficiencies.

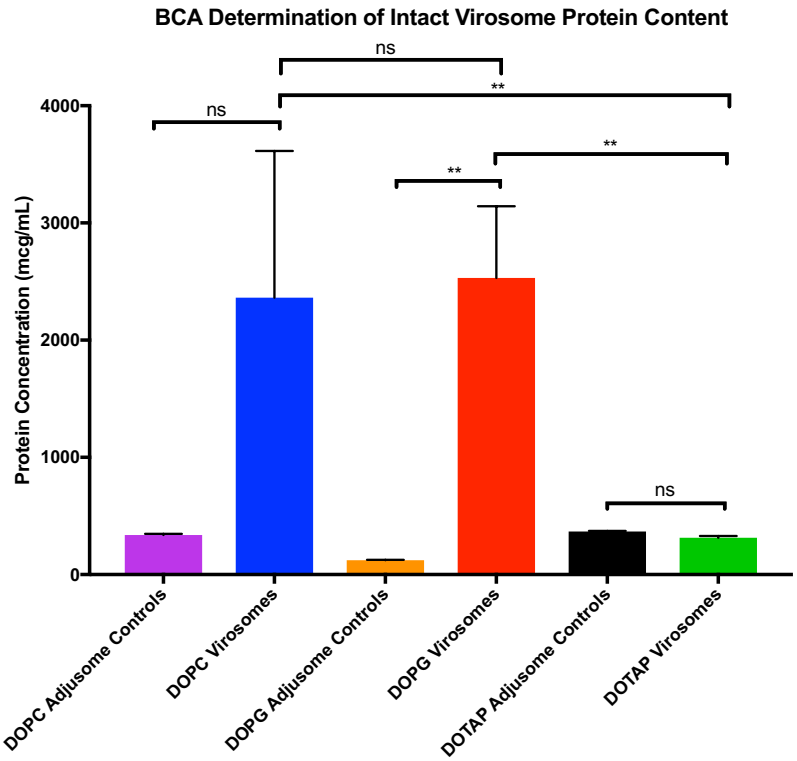

Figure 24. Summary of total protein content of intact virosomes as determined by BCA assay. Quantification of external total protein content reveals appreciable protein content in DOPC and DOPG virosomes, with minimal response observed in DOTAP virosomes. Values equal mean $\pm$ standard deviation (virosomes: n=9; liposome controls: n=3). P-value: ** $\leq$ 0.01, ns = not significant.

Tabulated Results

This study aimed to evaluate three different cholesterol-lipid virosome ionic formulations for the relative incorporation of adjuvants, antigen, chemokine, and influenza A membrane proteins. The adjuvant and protein content results are summarized in Table 4, with greatest values highlighted in bold and italic:

Table 4. Summary of virosomal component content across all assays conducted.

Content	DOPC Virosomes	DOPG Virosomes	DOTAP Virosomes
MPLA (EU/mL)	589.2 ± 401.8	***986.1 ± 654.4***	0.100 ± 0.05074
OxPAPC ELISA (ABS)	0.35 ± 0.024	***0.36 ± 0.016***	0.14 ± 0.007
OxPAPC SEC (Area)	978.2 ± 222.1	***2753 ± 421.8***	0 ± 0
GM-CSF (ng/mL)	766.2 ± 448.1	***1537 ± 40.17***	89.47 ± 11.93
ErbB2 (mcg/mL)	***6.905 ± 0.437***	5.581 ± 1.331	4.9 ± 1.536
NA MUNANA (AFUs)	57532 + 11445	***68235 ± 6748***	10142 ± 3370
NA SEC (Area)	25.59 ± 24.78	***427.7 ± 111.7***	0 ± 0
Intact HA (mcg/mL)	591.7 ± 217.9	305.6 ± 80.83	***1067 ± 172***
Disrupted HA (mcg/mL)	1154 ± 403.4	478.3 ± 60.38	***1212 ± 213.5***

Summary of content values across virosomal formulations. Values equal mean ± standard deviation.

Chapter V

Discussion

Liposomes have a long history in small molecule drug delivery for fungal and cancer applications, however their use in vaccination is only now starting to see clinical use. Currently, there are two marketed liposome-based vaccine products, Epaxal, against the hepatitis A virus, and Inflexal, an influenza vaccine, in contrast to ten approved fungal and cancer therapies (Bulbake, 2017). Recent liposome-based vaccine approaches have explored adhesion and/or encapsulation of adjuvant and antigen combinations (Schwendener, 2014), including the incorporation of the adjuvant MPLA (Konur, 2008). Other studies have examined the ability to incorporate membrane proteins into liposomes, primarily using membrane proteins derived from detergent disrupted cells, to produce proteoliposomes (Rigaud, 2003). This study extended these liposome-based approaches to produce virosomes incorporating recombinant HA and NA, without the need for detergent, in combination with lipophilic adjuvants to further potentiate vaccination against encapsulated ErbB2 antigen. This would be anticipated to stimulate both innate and adaptive immune responses using a single nanoparticle structure.

This study successfully demonstrated the ability to manufacture and characterize a complex, eight component virosome technology. The incorporation of six bioactive compounds into three different liposome formulations (anionic, neutral, and cationic) through the use of a liposome thin film rehydration production process was evaluated.

Both anionic virosomes formulated with DOPG and a neutral formulation using DOPC were found to incorporate all six compounds. Cationic virosomes formulated with DOTAP were found to incorporate minimal quantities of GM-CSF, NA, OxPAPC, and MPLA, suggesting that lipid charge had significant influence on incorporation efficiencies. As summarized in Table 4, DOPG virosomes were found to incorporate the greatest content for NA, GM-CSF, OxPAPC and MPLA constituents. DOPC and DOTAP virosomes were found to have greater ErbB2 and HA content, respectively. Both DOPC and DOPG virosomes were shown to be stable through 28 days in 10% sucrose, 20 mM HEPES, pH 7.3 as determined by dynamic light scattering. With the formulation and production approach used here, DOPG virosomes were identified as the lead candidate for potential further development. The thin film rehydration process used is a simple and rapid production technique that could enable the additional studies required to optimize this technology for further *in vivo* work and potential clinical translation.

Cationic (DOTAP) liposomes are traditionally used as vaccine adjuvants as the abundant positive charges on the surface can interact with anionic mammalian cell membranes, facilitating cellular uptake (Schwendener, 2014) and production of pro-inflammatory cytokines (Lonez, 2012). The failure to incorporate NA, GM-CSF, OxPAPC, and MPLA into DOTAP liposomes indicates that this configuration would require further formulation development to potentially obtain acceptable incorporation. However, it is noted that the immune stimulatory effects of cationic liposomes may not be required in this system due to the high immunogenicity of HA and the immune-stimulatory effects of incorporated adjuvants. While anionic and neutral liposomes are poorly immunogenic and anionic formulations may be electrostatically repulsive to cell

membranes, the incorporation of externally displayed HA and NA should be anticipated to alleviate these shortcomings through fusogenicity and protein mediated steric hindrance between liposomes, respectively.

Conventional protein liposome loading efficiencies can range between ~20 to ~80%, depending on the protein and liposome formulation (Anderson, 1994). The relatively low protein incorporation efficiencies observed across all formulations in this study is likely the result of the manufacturing process employed. The thin film rehydration process was selected for these studies due to its high protein compatibility, however it is known to produce relatively low encapsulation efficacies (Popovska, 2013). This rehydration process often requires sonication and heating during extrusion, manipulations capable of denaturing proteins during extended periods of exposure. To minimize potential protein denaturation, the rehydration procedure was modified to exclude the use of heat during extrusion, while limiting sonication pulses to one second intervals. Given these concerns, ELISAs and the MUNANA activity assay were utilized across all protein content determinations to provide a surrogate determination of bioactivity. These methods require intact tertiary protein structures for positive results in each assay, therefore results reported reflect native/active protein content.

The critical virosomal fusion component, hemagglutinin, was shown to be displayed on the exterior of the lipid bilayer across all three liposome formulations, suggesting that this production technique could be extended further to the incorporation of active HA to produce biologically active virosomes. While other approaches to incorporate HA onto liposomes have used either ionic interactions (Barnier-Quer, 2013) or lipid-conjugation (Kemble, 1994) for instance, these approaches could potentially limit

fusogenicity through improper orientation of the catalytic active site or potential denaturation, respectively. This study suggests that HA was incorporated through the membrane binding domain, as substantiated by the observation that the intact virosome HA ELISA found relatively comparable HA content across all lipid charge formulations suggesting a minimal influence of charge on HA incorporation. In addition, HA (A/California/04/2009) has an isoelectric point of 7.3, suggesting that the protein would be close to neutral in the Sucrose/HEPES, pH 7.3 reconstitution solution (Zhang, 2017), thus minimizing potential ionic interactions. With the potential incorporation of bioactive HA, these virosomes could enable the activation of the adaptive immune system through MHC I presentation of antigen.

The influenza membrane glycoprotein NA and the damage associated molecular pattern OxPAPC were also found to be displayed on the exterior of the lipid bilayer in DOPC and DOPG virosome formulations. The external presentation of NA, and HA, suggests that the virosomes produced resemble those generated using conventional virosome production methods. However, as this study incorporated recombinant influenza membrane proteins, these synthetic virosomes have a significantly reduced safety profile compared to conventional virosomes produced from live viruses, which may contain residual genetic material capable of enabling viral replication. The external presentation of OxPAPC, in conjunction with MPLA incorporation would be expected to provide a strong stimulation of the innate immune system by mimicking an extreme infection (Zanoni, 2016).

The ability to stimulate both the innate and adaptive immune systems utilizing a rapidly produced synthetic virosome, in conjunction with the encapsulation of the antigen

ErbB2 and the DC recruiting cytokine GM-CSF represents a powerful nanoparticle. Here, a single structure may be capable of dendritic cell recruitment, potent stimulation of the immune system, and delivery of native ErbB2 protein for MHC I processing. Further, inclusion of these components into a lipid-based nanoparticle is anticipated to increase the half-life of encapsulated proteins, while reducing potential off target toxicities of incorporated adjuvants. Finally, these virosomes may be combined with other technologies, such as hydrogels, to increase residency time and enhance for dendritic cells to the site of administration.

This research indicates that an *ex vivo* recombinant-protein based virosomes can be successfully produced using a thin film rehydration method. Given the complexity of this vaccine configuration, incorporation of all components in two of three lipid formulations represents a significant accomplishment. Virosome production using recombinant proteins presents a major step forward toward in the reduction of safety concerns associated with these virus-like nanoparticles. Considering the platform nature of this technology, this approach could be applicable to the loading of other antigens, thus enabling vaccination against a broader spectrum of disease conditions. Further, these nanoparticles could be utilized for both vaccination, as presented in this configuration, or for cytosolic drug delivery, thus significantly expanding its potential application.

Previous research efforts have largely sought to elicit immune responses through the mixture of paired antigen and adjuvant combinations (Schwendener, 2014). The flexibility of this approach, affords the opportunity to quickly screen new antigen targets, novel adjuvants, immune-modulating cytokine/chemokines, and combinations thereof as exemplified here - features critical to the advancement of clinical cancer treatment

strategies. The successful incorporation of six bioactive components into a lipid-based nanoparticle, as reported here, represents a significant increase in complexity and should be expected to lead to a potent MHC I vaccine. Combinatorial products appear to be the future of cancer medicine, where multi-faceted approaches are utilized to combat the ever-evolving challenge that is oncotherapy. This study hopes to serve as a stepping stone towards that end.

Appendix 1

Definition of Terms

Adjuvant: A chemical species that potentiates the immune response against an antigen.

Antigen: A chemical, peptide, protein, saccharide, etc. that an elicits an immune response.

CAR-T: Chimeric Antigen-Receptor modified T-cells.

$CD4^+$ T-cells: T-helper cells aid in the activation and differentiation of memory cells and plasma cells (antibody generating cells).

$CD8^+$ T-cells/CTLs: Cytotoxic T (lymphocytes) cells responsible for the killing of viruses, bacterial infections, and cancer.

CTLA-4: Cytotoxic T-Lymphocyte-Associated Protein 4

DCPC: 1,2 dihexanoyl-*sn*-glycero-3-phosphocholine

DLS: Dynamic Light Scattering

DOTAP: 1,2-di-(9Z-octadecenoyl)-3-trimethylammonium-propane (chloride salt)

DOPC: 1,2-di-(9Z-octadecenoyl)-*sn*-glycero-3-phosphocholine

DOPG: 1,2-di-(9Z-octadecenoyl)-*sn*-glycero-3-phospho-(1'-*rac*-glycerol) (sodium salt)

ELISA: Enzyme-Linked Immunosorbent Assay

Endocytosis: The process by which cells will intake material through invagination of the cell membrane.

GPC: Gel Permeation Chromatography

HPLC: High Performance Liquid Chromatography

Hydrogel: A polymer based, ionically or covalently cross-linked network that is mostly water.

Inflammasome: A multi-protein complex that activates the inflammatory process as part of the innate immune response.

Kaplan-Meier Survival Curve: A plot often used in medicine to depict patient survival as a function of time.

LPS: Lipopolysaccharide (bacterial endotoxin)

Major Histocompatibility Complex (MHC): Cell surface proteins capable of displaying antigens as part of the acquired immune system.

Multilamellar: A liposome structure containing multiple, concentric, lipid bilayers.

Neoplastic: Abnormal growth of cells or tissue; a malignant or benign tumor.

OxPAPC: Oxidized 1-palmitoyl-2-arachidonyl-*sn*-glycero-3-phosphorylcholine

PD-1: Programmed Cell Death Protein 1, a transmembrane receptor found on activated T-Cells that is an immune check point, where is it thought to play a major role in the regulation of immune response to self-tolerance.

PDL-1: Programmed Cell Death Ligand 1, a transmembrane protein found on antigen presenting cells that upon binding with PD-1 acts to inhibit T-Cell proliferation.

PolyDispersity Index (PDI): A measure of the distribution of particle size within a sample.

Pyroptosis: A highly inflammatory version of programmed cell death commonly found in association with bacterial infection.

Unilamellar: A liposome structure containing one lipid bilayer.

Appendix 2

Size by dynamic light scattering profiles of adjusomes pre-dialysis and post-dialysis across PBS and Sucrose/HEPES rehydration formulations.

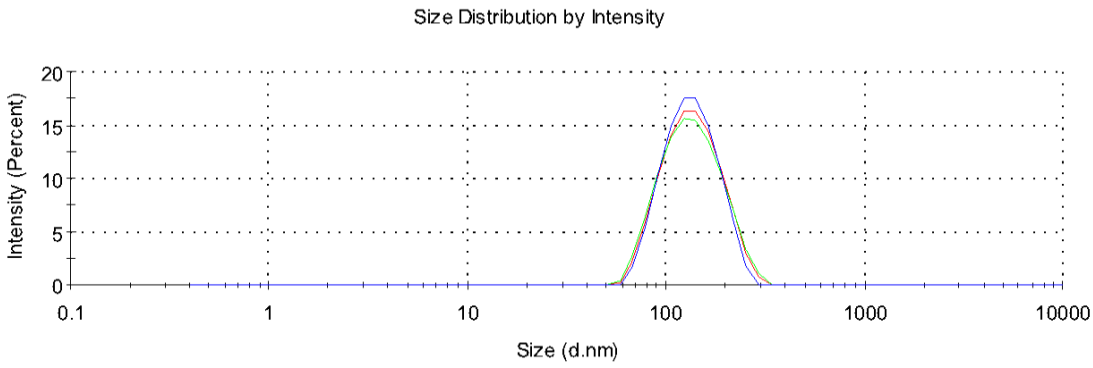

Supplemental Figure1. Representative size distribution of DOPC adjusomes reconstituted in PBS post-extrusion and pre-dialysis.

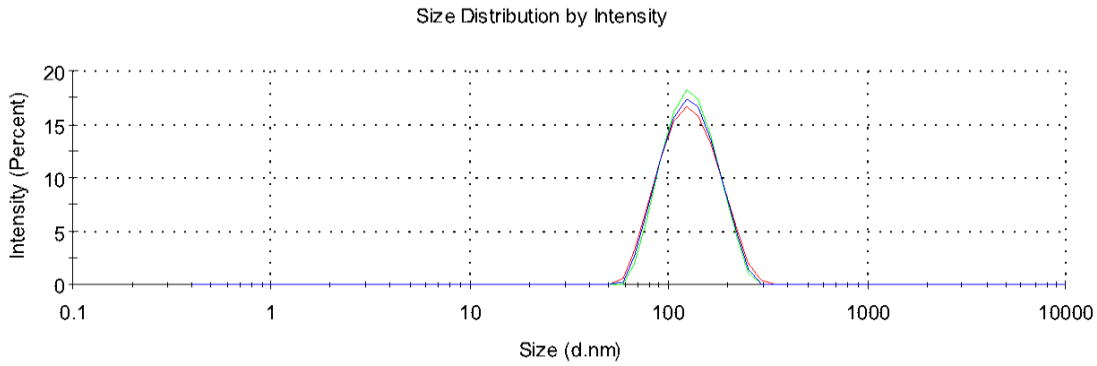

Supplemental Figure 2. Representative size distribution of DOPG adjusomes reconstituted in PBS post-extrusion and pre-dialysis.

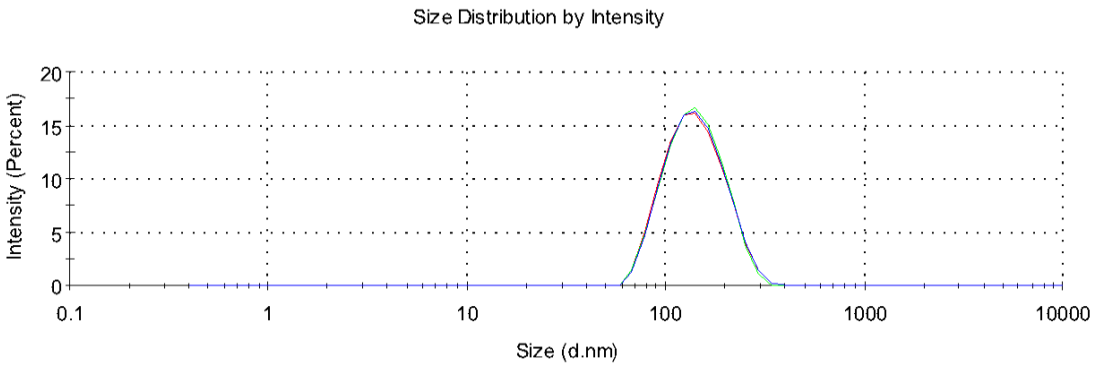

Supplemental Figure 3. Representative size distribution of DOTAP adjusomes reconstituted in PBS post-extrusion and pre-dialysis.

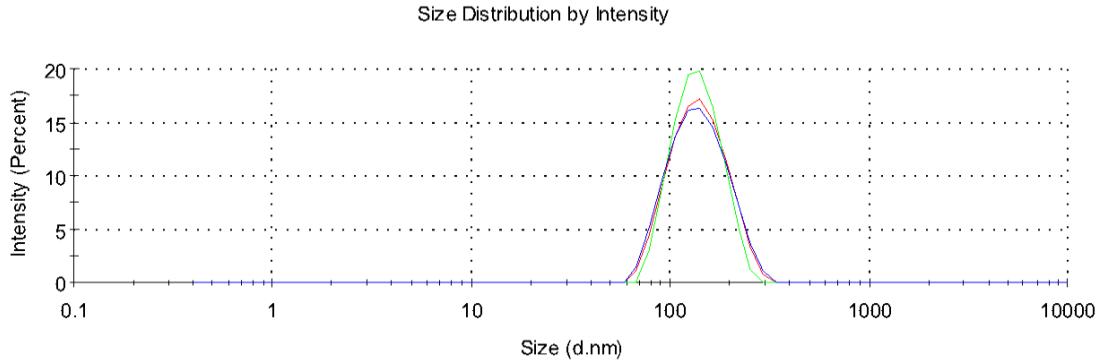

Supplemental Figure 4. Representative size distribution of DOPC adjusomes reconstituted in 10% Sucrose, 20 mM HEPES, pH 7.3 post-extrusion and pre-dialysis.

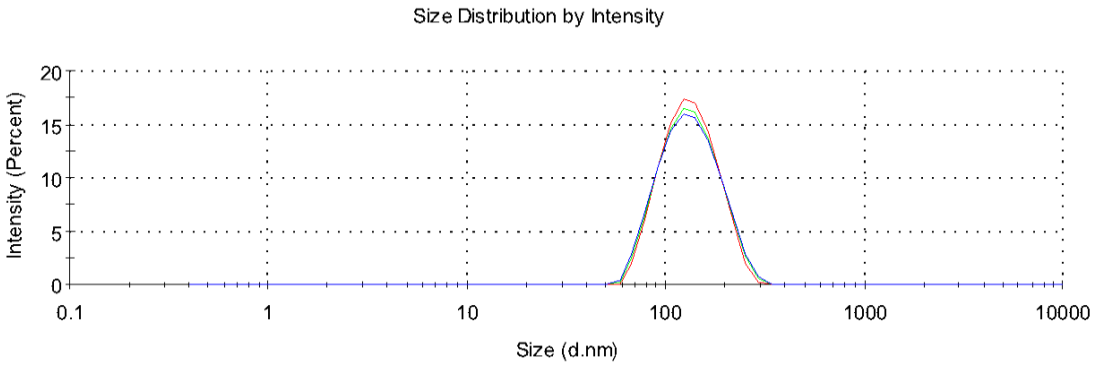

Supplemental Figure 5. Representative size distribution of DOPG adjusomes reconstituted in 10% Sucrose, 20 mM HEPES, pH 7.3 post-extrusion and pre-dialysis.

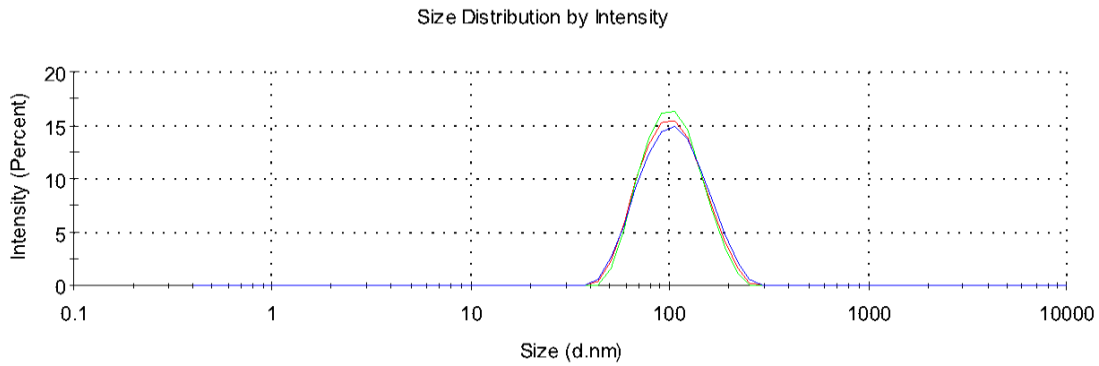

Supplemental Figure 6. Representative size distribution of DOTAP adjusomes reconstituted in 10% Sucrose, 20 mM HEPES, pH 7.3 post-extrusion and pre-dialysis.

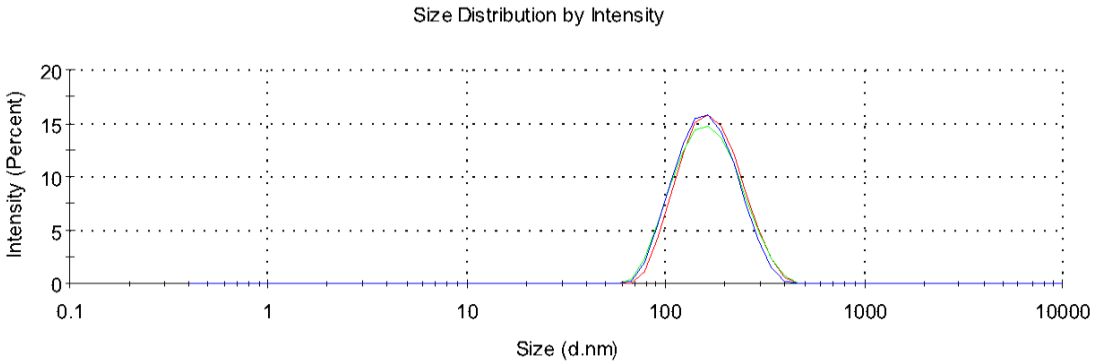

Supplemental Figure 7. Representative size distribution of DOPC adjusomes reconstituted in PBS post-extrusion and post-dialysis.

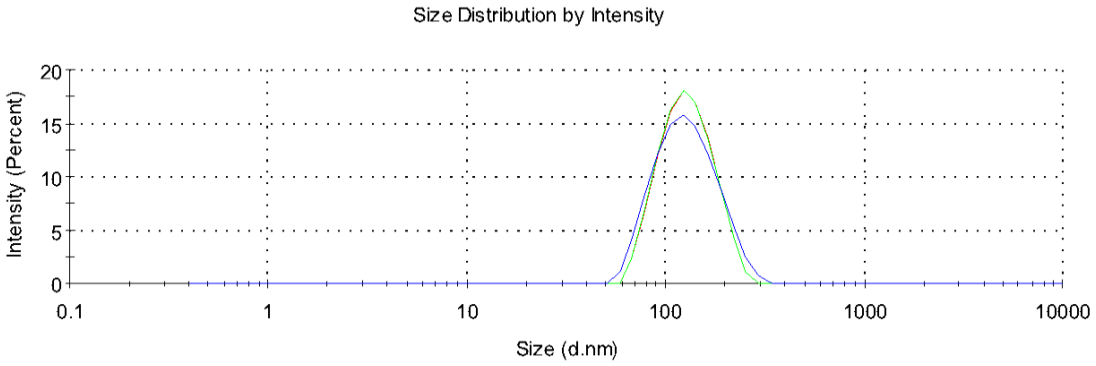

Supplemental Figure 8. Representative size distribution of DOPG adjusomes reconstituted in PBS post-extrusion and post-dialysis.

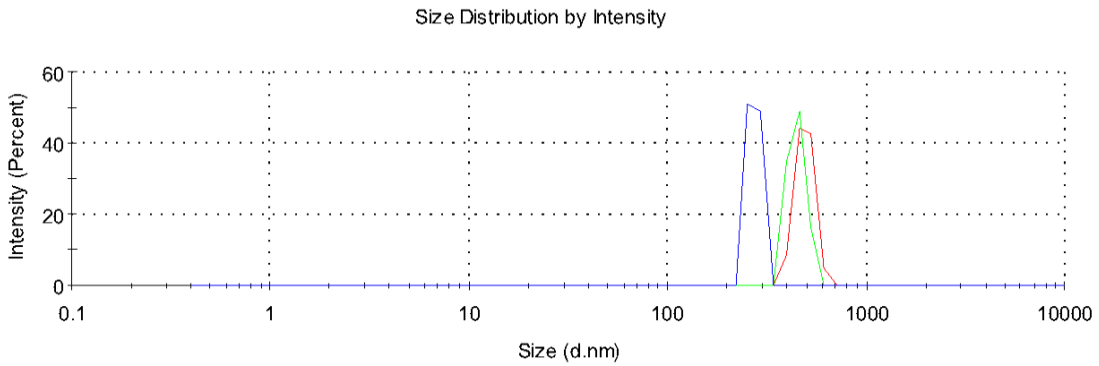

Supplemental Figure 9. Representative size distribution of DOTAP adjusomes reconstituted in PBS post-extrusion and post-dialysis.

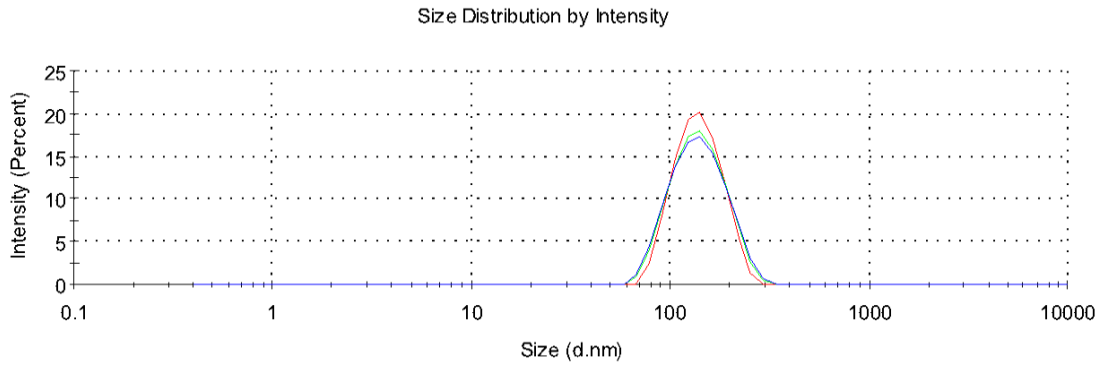

Supplemental Figure 10. Representative size distribution of DOPC adjusomes reconstituted in 10% Sucrose, 20 mM HEPES, pH 7.3 post-extrusion and post-dialysis.

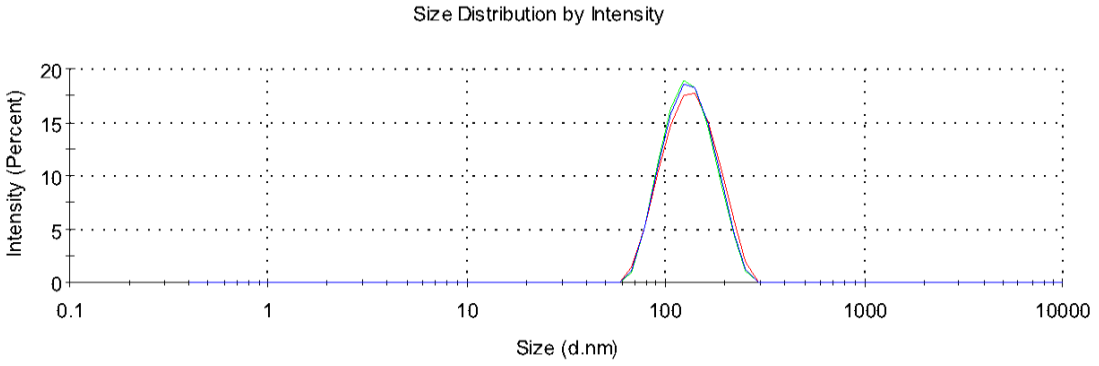

Supplemental Figure 11. Representative size distribution of DOPG adjusomes reconstituted in 10% Sucrose, 20 mM HEPES, pH 7.3 post-extrusion and post-dialysis.

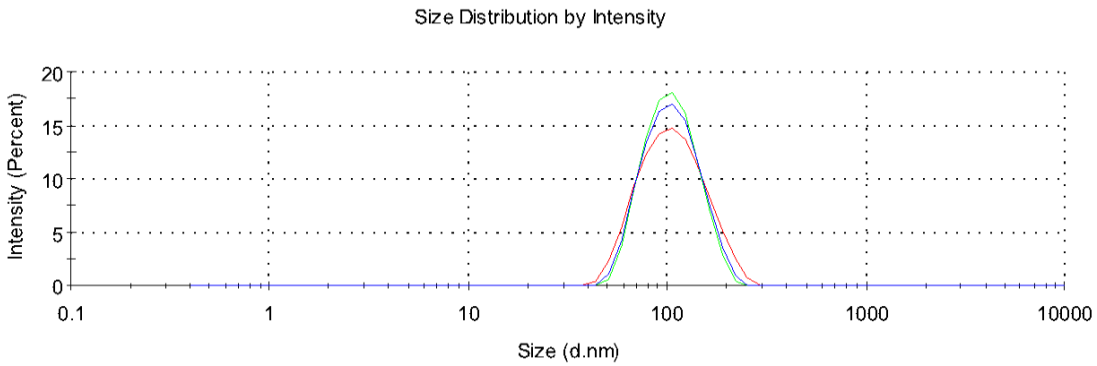

Supplemental Figure 12. Representative size distribution of DOTAP adjusomes reconstituted in 10% Sucrose, 20 mM HEPES, pH 7.3 post-extrusion and post-dialysis.

Appendix 3

Size by dynamic light scattering profiles of virosomes pre-dialysis, post-dialysis, and 7-day stability.

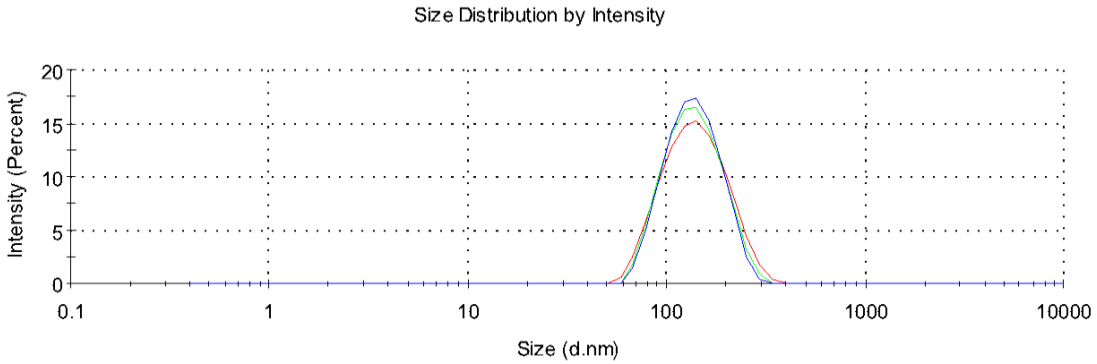

Supplemental Figure 13. Representative size distribution of DOPC virosomes reconstituted in Sucrose/HEPES post-extrusion and pre-dialysis.

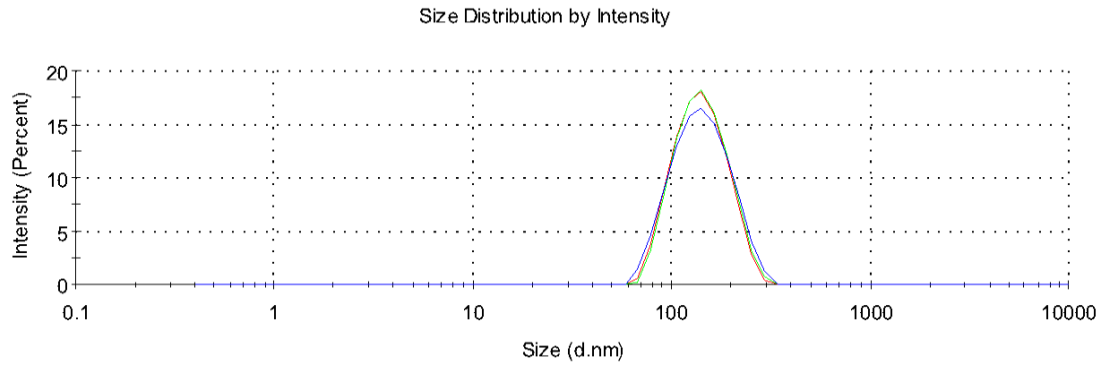

Supplemental Figure 14. Representative size distribution of DOPG virosomes reconstituted in Sucrose/HEPES post-extrusion and pre-dialysis.

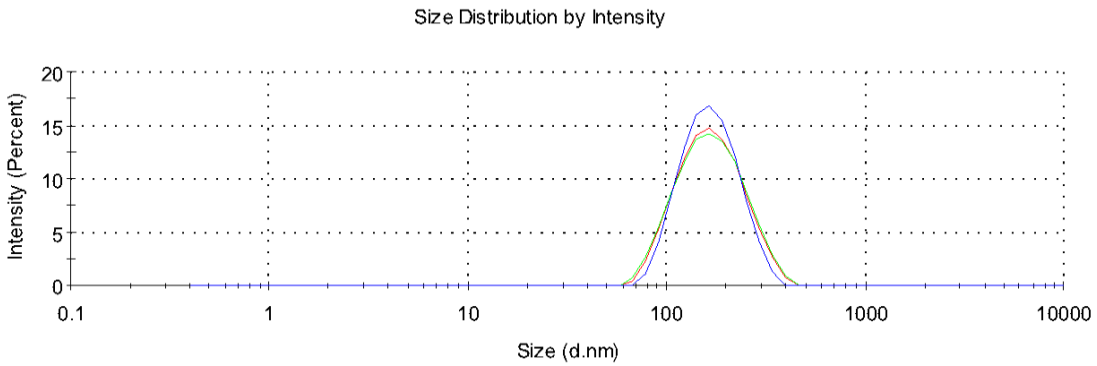

Supplemental Figure 15. Representative size distribution of DOTAP virosomes reconstituted in Sucrose/HEPES post-extrusion and pre-dialysis.

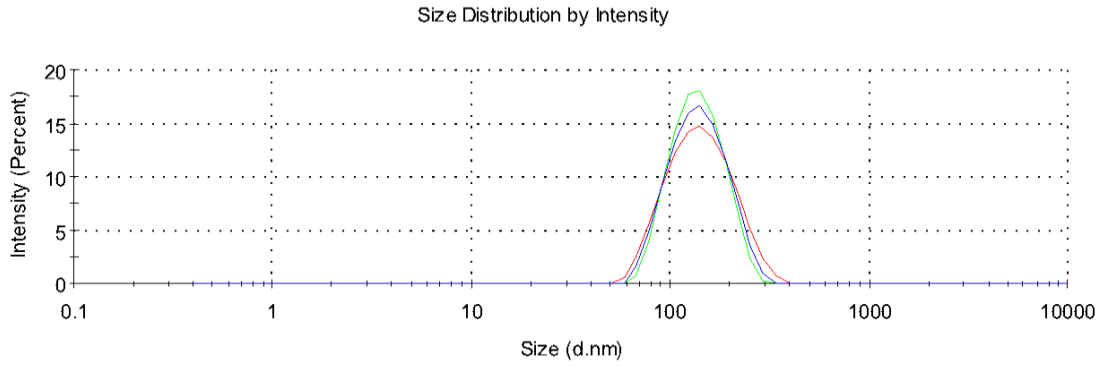

Supplemental Figure 16. Representative size distribution of DOPC virosomes reconstituted in Sucrose/HEPES post-extrusion and post-dialysis.

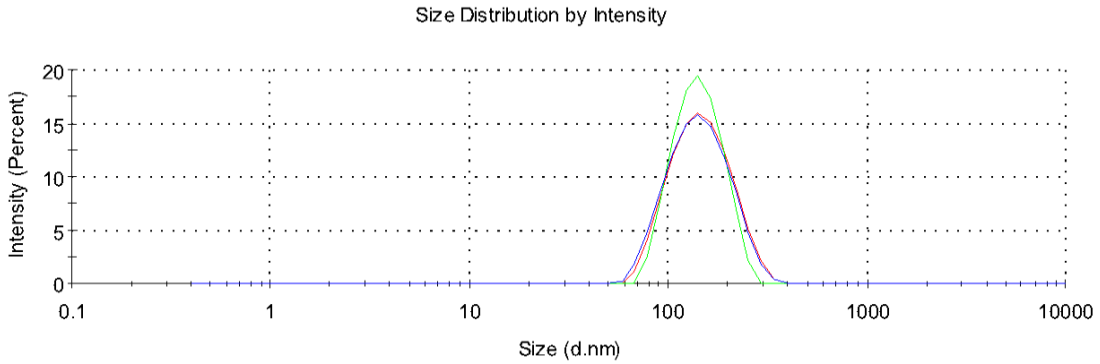

Supplemental Figure 17. Representative size distribution of DOPG virosomes reconstituted in Sucrose/HEPES post-extrusion and post-dialysis.

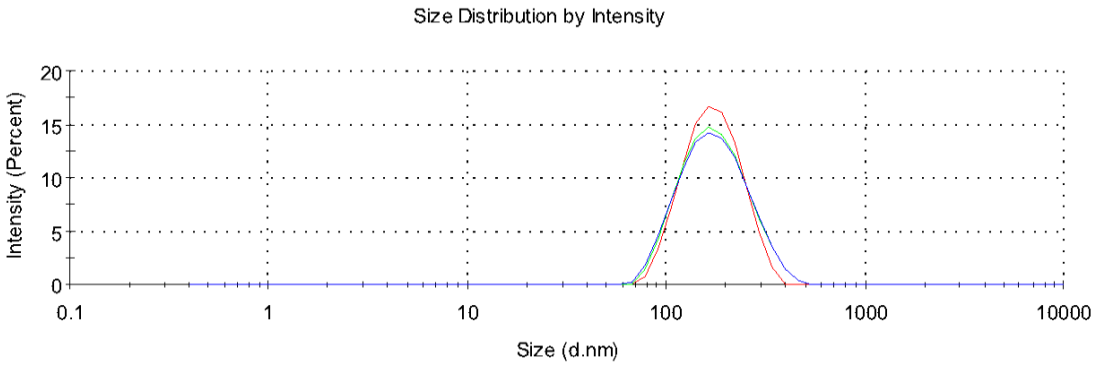

Supplemental Figure 18. Representative size distribution of DOTAP virosomes reconstituted in Sucrose/HEPES post-extrusion and post-dialysis.

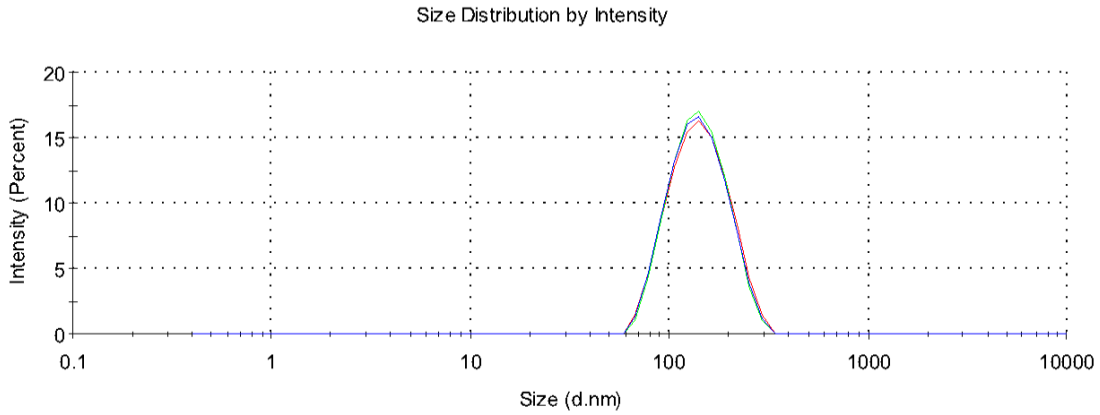

Supplemental Figure 19. Representative size distribution of DOPC virosomes reconstituted in Sucrose/HEPES post-extrusion and post-dialysis – 7-day stability.

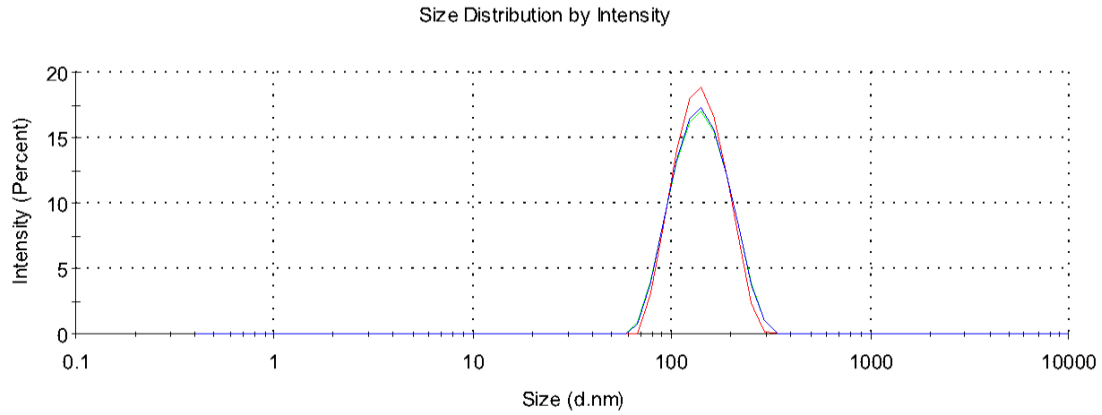

Supplemental Figure 20. Representative size distribution of DOPG virosomes reconstituted in Sucrose/HEPES post-extrusion and post-dialysis – 7-day stability.

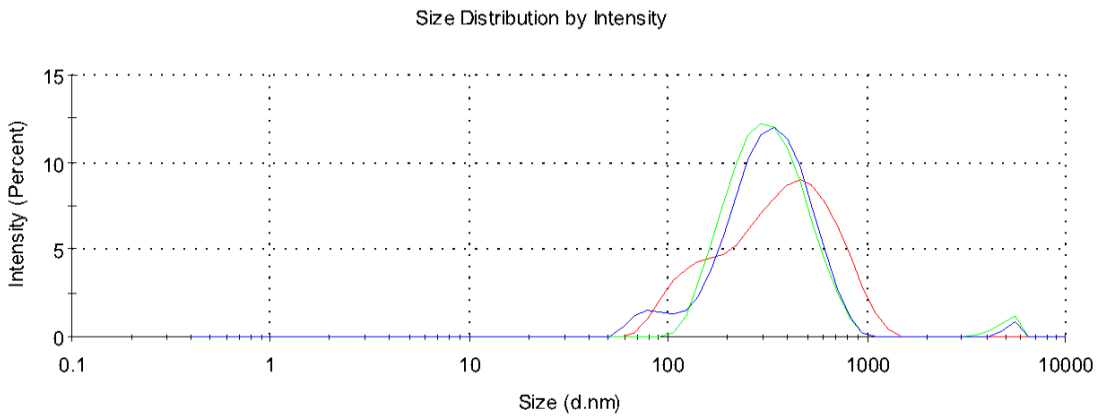

Supplemental Figure 21. Representative size distribution of DOTAP virosomes reconstituted in Sucrose/HEPES post-extrusion and post-dialysis – 7-day stability.

Appendix 4

Molecular Structures of Lipid Components

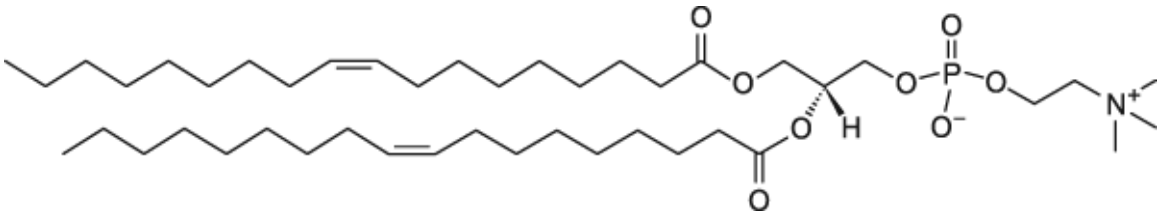

Supplemental Figure 22. Molecular structure of DOPC: 1,2-di-(9Z-octadecenoyl)-*sn*-glycero-3-phosphocholine
Retrieved from: https://avantilipids.com/product/850375/

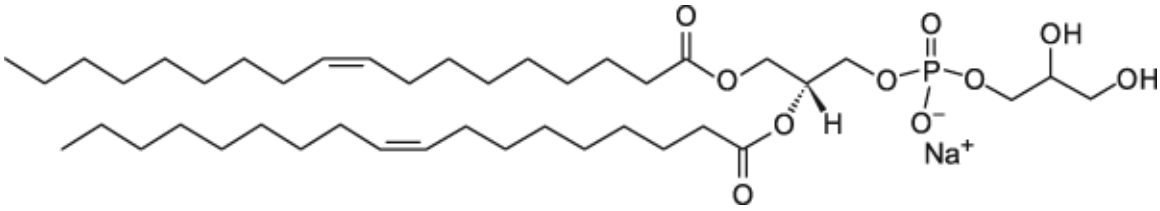

Supplemental Figure 23. Molecular structure of DOPG: 1,2-di-(9Z-octadecenoyl)-*sn*-glycero-3-phospho-(1'-*rac*-glycerol) (sodium salt)
Retrieved from: https://avantilipids.com/product/840475/

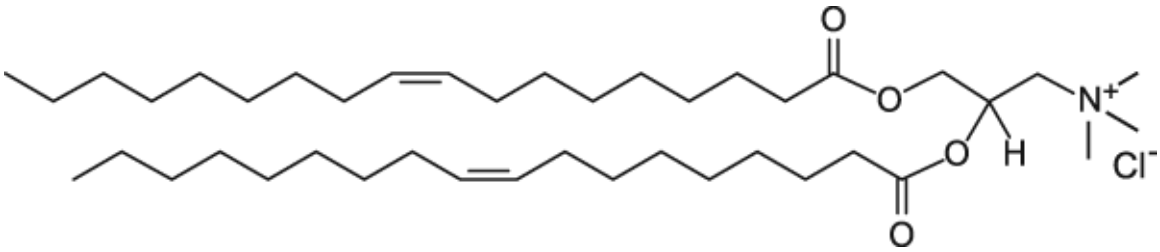

Supplemental Figure 24. Molecular structure of DOTAP: 1,2-di-(9Z-octadecenoyl)-3-trimethylammonium-propane (chloride salt)
Retrieved from: https://avantilipids.com/product/890890/

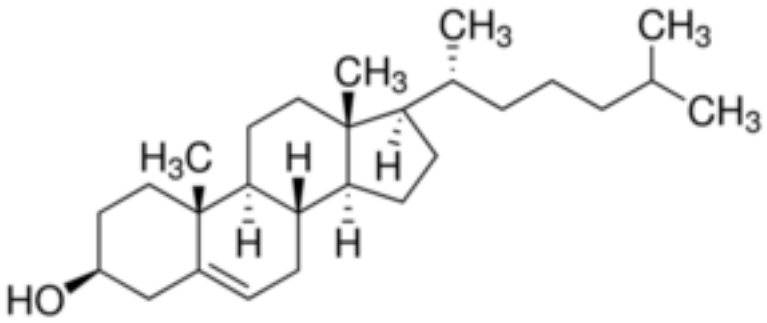

Supplemental Figure 25. Molecular structure of Cholesterol.
Retrieved from: http://www.sigmaaldrich.com/catalog/product/sigma/c8667

Appendix 5

Molecular Structure of MUNANA

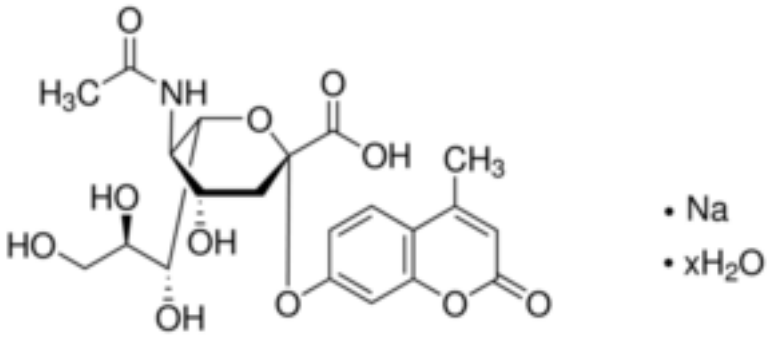

Supplemental Figure 26. Molecular structure of 2′-(4-Methylumbelliferyl)-α-D-*N*-acetylneuraminic acid (MUNANA).
Retrieved from: http://www.sigmaaldrich.com/catalog/product/sigma/m8639

Appendix 6

Schematic of Thin Film Rehydration

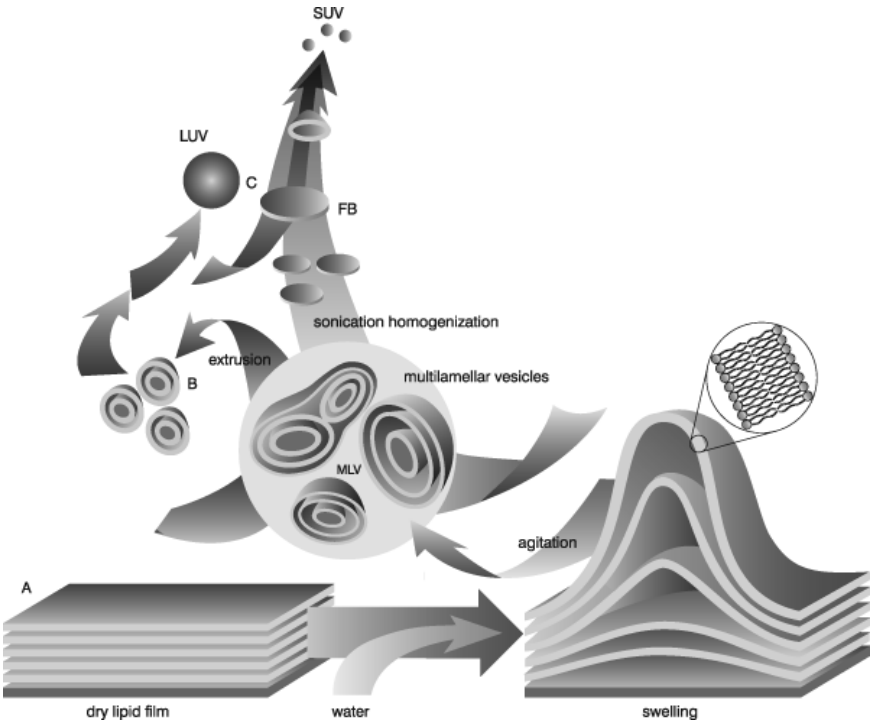

Supplemental Figure 27. Schematic illustrating liposome production through thin film rehydration.
Retrieved from: https://avantilipids.com/tech-support/liposome-preparation/

References

Abdoli, A., Soleimanjahi, H., Kheiri, M. T., Jamali, A., Sohani, H., Abdoli, M., & Rahmatollahi, H. R. (2013). Reconstitution of H_3N_2 influenza virus based virosome in-vitro. *Iranian Journal of Microbiology, 5*(2), 166-171.

Adamina, M., Guller, U., Bracci, L., Heberer, M., Spagnoli, G. C., & Schumacher, R. (2006). Clinical applications of virosomes in cancer immunotherapy. *Expert Opinion on Biological Therapy, 6*(11), 1113-1121.

Ali, O. A., Huebsch, N., Cao, L., Dranoff, G., & Mooney, D. J. (2009). Infection-mimicking materials to program dendritic cells *in situ*. *Nature Materials, 8*, 151-158.

Anderson, P. M., Hanson, D. C., Hasz, D. E., Halet, M. R., Blazar, B. R., & Ochoa, A. C. (1994). Cytokines in liposomes: Preliminary studies with IL-1, IL-2, IL-6, GM-CSF and Interferon-γ. *Cytokine, 6*(1), 92-101.

Banchereau, J., Briere, F., & Caux, C. (2000). Imunnobiology of dendritic cells. *Annual Review of Immunology, 18*, 767-811.

Barnier-Quer, C., Elsharkawy, A., Romeijn, S., Kros, A., & Jiskoot, W. (2013). Adjuvant effect of cationic liposomes for subunit influenza vaccine: Influence of antigen loaded method, cholesterol, and immune modulators. *Pharmaceutics, 5*, 392-410.

Blut, A. (2009). Influenza virus. *Transfusion Medicine and Hemotherapy, 36*, 32-39.

Bouhadir, K. H., Lee, K. Y., Alsberg, E., Damm, K. L., Anderson, K. W., & Mooney, D. J. (2001). Degradation of partially oxidized alginate and its potential application for tissue engineering. *Biotechnology Progress, 17*, 945-950.

Bulbake, U., Doppalapudi, S., Kommineni, N., & Khan, W. (2017). Liposomal formulations in clinical use: An updated review. *Pharmaceuticals, 9*(12), doi:10.3990/pharmaceuticals9020012

Bungener, L., Serre, K., Bijl, L., Leserman, L., Wilschut, J., Daemen, T., & Machy, P. (2002). Virosome-mediated delivery of protein antigens to dendritic cells. *Vaccine, 20*(17-18), 2287-2295.

Casella, C. R., & Mitchell, T. C. (2008). Putting endotoxin to work for us: monophosphoryl lipid A as a safe and effective vaccine adjuvant. *Cellular and Molecular Life Sciences, 65*(20), 3231-3240.

Chen, J., Lee, K. H., Steinhauer, D. A., Stevens, D. J., Skehel, J. J., & Wiley, D. C. (1998). Structure of the hemagglutinin precursor cleavage site, a determination of influenza pathogenicity and the origin of the labile conformation. *Cell, 95*, 409-417.

Clogston J. D., & Patri A. K. (2011). Zeta potential measurement. In: McNeil S. (eds), *Characterization of nanoparticles intended for drug delivery. Methods in molecular biology (methods and protocols), volume* 697 (pp. 63-70). New York, NY: Humana Press.

Coffman, R. L., Sher, A. & Seder, R. A. (2010). Vaccine adjuvants: Putting innate immunity to work. *Immunity, 33*(4), 492-503.

Desai, R. M., Koshy, S. T., Hilderbrand, S.A., Mooney, D. J., & Joshi, N. S. (2015). Versatile click alginate hydrogels crosslinked via tetrazine-norbornene chemistry. *Biomaterials, 50*, 30-37.

Dijkstra, J., Bron, R., Wilschut, J., de Haan, A., & Ryan, J. L. (1996). Activation of murine lymphocytes by lipopolysaccharide incorporated in fusogenic, reconstituted influenza virus envelopes (virosomes). *Journal of Immunology, 157*, 1028-1036.

Drury, J. L., & Mooney, D. J. (2003). Hydrogels for tissue engineering: scaffold design variables and applications. *Biomaterials, 24*, 4337-4351.

Dua, J. S., Rana, A. C., Bhandrai, A. K. (2012). Liposome: Methods of preparation and applications. *International Journal of Pharmaceutical Studies and Research, 3*(2), 14-20.

Dranoff, G., Jaffee, E., Lazenby, A., Golumbek, P., Levitsky, H., Brose, K., ... Mulligan, R. C. (1993). Vaccination with irradiated tumor cells engineered to secrete murine granulocyte-macrophage colony-stimulating factor stimulates potent, specific, and long-lasting anti-tumor immunity. *Proceedings of the National Academy of Sciences, 90*, 3539–3543.

Felnerova, D., Viret, J. F., Glück, R., & Moser, C. (2004). Liposomes and virosomes as delivery systems for antigens, nucleic acids and drugs. *Current Opinion in Biotechnology, 15*, 518-529.

Engvall, E., & Perlmann, P. (1971). Enzyme-linked immunosorbent assay (ELISA) quantitative assay of immunoglobulin G. *Immunochemistry*, *8*(9), 871-874.

Gee, A. P., Sumstad, D., Stanson, J., Watson, P., Proctor, J., Kadidlo, D., ... Lindblad, R. (2008). A multi-center comparison study between the EndoSafe PTS rapid release testing system and traditional test methods for detecting endotoxin in cell therapy products. *Cytotherapy, 10*(4), 427-435.

Greenwood, B. (2014). The contribution of vaccination to global heath: past, present and future. *Philosophical Transactions of the Royal Society B, 369*, 20130433. doi:10.1098/rstb.2013.0433.

Grijalvo, S., Mayr, J., Eritja, R., & Diaz Diaz, D. (2016). Biodegradable liposome-encapsulating hydrogels for biomedical applications: a marriage of convenience. *Biomaterials Science, 4*, 555-574.

Harrington, K.J., Rowlinson-Busza, G., Syrigos, K. N., Uster, P. S., Vile, R. G., & Stewart, J. S. W. (2000). Pegylated liposomes have potential as vehicles for intratumoral and subcutaneous drug delivery. *Clinical Cancer Research, 6*(6), 2528-2537.

Hassan, P. A., Rana, S., & Verma, G. (2015). Making sense of brownian motion: Colloid characterization by dynamic light scattering. *Langmuir*, *31*, 3-12.

Hodi, F. S., O'Day, J., McDermott, D. F., Weber, R. W., Sosman, J. A., Haanen, J. B., ... Urba, W. J. (2010). Improved survival with Ipilimumab in patients with metastatic melanoma. *New England Journal of Medicine, 363*, 711-723.

Hong, P., Koza, S., & Bouvier, E. S. P. (2012). Size-exclusion chromatography for the analysis of protein biotherapeutics and their aggregates. *Journal of Liquid Chromatography and Related Technologies, 35*(20), 2923-2950.

Kaneda, Y. (2000) Virosomes: evolution of the liposome as a targeted drug delivery system. *Advanced Drug Delivery Reviews. 43*(2-3): 197-205.

Kemble, G. W., Danieli, T., & White, J. M. (1994). Lipid-anchored influenza hemagglutinin promotes hemifusion, not complete fusion. *Cell, 76*, 383-391.

Klenk, H. D., Rott, R., Orlich, M., & Blodorn, J. (1975). Activation of influenza A viruses by trypsin treatment. *Virology, 68*, 426-439.

Klenk, H. D., & Garten, W. (1994). Host cell proteases controlling virus pathogenicity. *Trends in Microbiology, 2*, 39-43.

Konur, A., Graser, A., Klamp, I., Kreiter, S., Selmi, A., Diken, M., ... Sahin, U. (2008). Liposome-encapsulated adjuvants are potent inducers of antigen specific T-Cells *in vivo*. *The Open Cancer Journal, 2*, 15-24

Lonez, C., Vandenbranden, M., & Ruysschaert, J. M. (2012). Cationic lipids activate intracellular signaling pathways. *Advanced Drug Delivery Reviews, 64*(15), 1749-1758.

New, R. R. C. (1994). *Liposomes as tools in basic research and industry.* Philippot, J.R., & Schuber, F. (Eds.). Boca Raton, FL: CRC Press, pp. 3-20.

Mach, N., & Dranoff, G. (2000). Cytokine-secreting tumor cell vaccines. *Current Opinion in Immunology, 12*, 571-575.

Mitri, Z., Constantine, T., & O'Regan, R. (2012). The HER2 receptor in breast cancer: Pathophysiology, clinical use, and new advances in therapy. *Chemotherapy Research and Practice*. doi:10.1155/2012/743193

Oblak, A., & Jerala, R. (2011). Toll-like receptor 4 activation in cancer progression and therapy. *Clinical and Developmental Immunology.* doi: 10.1155/2011/609579.

Olson, B. J. S. C, & Markwell, J. (2007). Assays for determination of protein concentration. *Current Protocols in Protein Science*. 3.4.1-3.4.29

Plotkin, S. (2014). History of vaccination. *Proceedings of the National Academy of Sciences, 111*(34), 12283-12287.

Popovska, O., Simonovska, J., Karakovski, Z., & Rafajlovska, V. (2013). An overview: Methods for preparation and characterization of liposomes as drug delivery systems. *International Journal of Pharmaceutical and Phytopharmacological Research, 3*(3), 182-189.

Potier, M., Mameli, L., Belisle, M., Dallaire, L., & Melancon, S. B. (1979). Fluorometric assay of neuraminidase with a sodium (4-methylumbelliferyl-α-D-N-acetylneuraminate) substrate. *Analytical Biochemistry, 94*, 287-296.

Rigaud, J. L., & Levy, D. (2003). Reconstitution of membrane proteins into liposomes. *Methods in Enzymology, 372*, 65-86.

Salazar, L. G., Fikes, J., Southwood, S., Ishioka, G., Knutson, K. L., Gooley, T. A., ... Disis, M. L. (2003). Immunization of cancer patients with HER-2neu-derived peptides demonstrating high-affinity binding to multiple class II alleles. *Clinical Cancer Research, 9,* 5559-5565.

Saroja, C. H., Lakshmi, P. K., & Bhaskaran, S. (2011). Recent trends in vaccine delivery systems: A review. *International Journal of Pharmaceutical Investigation, 1*(2), 64-74.

Schwendener, R. A. (2014). Liposomes as vaccine delivery systems: A review of the recent advances. *Therapeutic Advances in Vaccines, 2*(6), 159-182.

Senne, D. A., Panigrahy, B., Kawaoka, Y., Pearson, J. E., Suss, J., Lipkin, M., ... Webster, R. G. (1996). Survey of the hemagglutinin (HA) cleavage site sequence of H5 and H7 avian influenza viruses: Amino acid sequence at the HA cleavage site as a marker of pathogenicity. *Avain Diseases, 40*, 425-437.

Serafini, P., Carbley, R., Noonan, K. A., Tan, G., Bronte, V., & Borrello, I. (2004). High-dose granulocyte-macrophage colony-stimulating factor-producing vaccines impair the immune response through the recruitment of myeloid suppressor cells. *Cancer Research, 64,* 6337-6343.

Shtyrya, Y. A., Mochalova, L. V., & Bovin, N. V. (2009). Influenza virus neuraminidase: Structure and function. *Acta Naturae, 1*(2), 26-32.

Skehel, J. J., Bayley, P. M., Brown, E. B., Martin, S. R., Waterfield, M. D., White, J. M., & Wilson, I. A. (1982). Changes in the conformation of influenza virus hemagglutinin at the pH optimum of virus-mediated membrane fusion. *Proceedings of the National Academy of Sciences, 79*, 968-972.

Talesh, G. A., Ebrahimi, Z., Badiee, A., Mansourian, M., Attar, H., Arabi, L., ... Jaafari, M. R. (2016). Poly (I:C)-DOTAP cationic nanoliposome containing multi-epitope HER2-derived peptide promotes vaccine-elicited anti-tumor immunity in a murine model. *Immunology Letters, 176*, 57-64.

Van de Laar, L., Coffer, P. J., & Woltman, A. M. (2012). Regulation of dendritic cell development by GM-CSF: Molecular control and implications for immune homeostasis and therapy. *Blood, 119*(15), 3383-3393.

Webster, R. G. & Rott, R. (1987). Influenza virus A pathogenicity: The pivotal role of hemagglutinin. *Cell, 50*, 665-666.

Wetherall, N. T., Trivedi, T., Zeller, J., Hodges-Savola, C., McKimm-Breschkin, J. L., Zambon, M., & Hayden, F. G. (2003). Evaluation of neuraminidase enzyme assays using different substrates to measure susceptibility of influenza virus clinical isolates to neuraminidase inhibitors: Report of the neuraminidase inhibitor susceptibility network. *Journal of Clinical Microbiology, 41*(2), 742-750.

Whitney, C. G., Zhou, F., Singleton, J., & Schuchat, A. (2014). Benefits from immunization during the vaccines for children program era – United States, 1994-2013. *Morbidity and Mortality Weekly Report, 63*(16), 352-355. Retrieved from https://www.cdc.gov/mmwr/preview/mmwrhtml/mm6316a4.htm

Wiley, D. C., & Skehel, J. J. (1987). The structure and function of the hemagglutinin membrane glycoprotein of influenza virus. *Annual Review of Biochemistry, 56*, 365-394.

Yadav, A. V., Murthy, M. S., Shete, A. S., & Sakhare, S. (2011). Stability aspects of liposomes. *Indian Journal of Pharmaceutical Education and Research, 45*(4), 402-413.

Yarden, Y. (2001). Biology of HER2 and its importance in breast cancer. *Oncology, 61*, 1-13.

Zanoni, I., Tan, Y., Di Gioia, M., Broggi, A., Ruan, J., Shi, J., ... Kagan, J. C. (2016) An endogenous caspase-11 ligand elicits interleukin-1 release from living dendritic cells. *Science, 352*(6290), 1232-1236.

Zarei, S., Schwenter, F., Luy, P., Aurrand-Lions, M., Morel, P., Kopf, M., ... Mach, N. (2009). Role of GM-CSF signaling in cell-based tumor immunization. *Blood, 113*, 6658-6668.

Zhang, Y., Aevermann, B. D., Anderson, T. K., Burke, D. F., Dauphin, G., Gu, Z., ... Scheuermann, R. H. (2017). Influenza research database: An integrated bioinformatics resource for influenza virus research. *Nucleic Acids Research, 4*(45:D1), D466-D474. Entry: https://www.fludb.org/brc/fluSegmentDetails.spg?ncbiGenomicAccession=KU933485&decorator=influenza